AD-A099 517 PERKIN-ELMER CORP NORWALK CONN F/G 20/12
GROWTH OF ALUMINUM GALLIUM NITRIDE THIN FILMS FOR ELECTRO-OPTIC--ETC(U
FEB 81 D L SMITH, R H BRUCE N00014-77-C-0492
UNCLASSIFIED PE-28935 NL

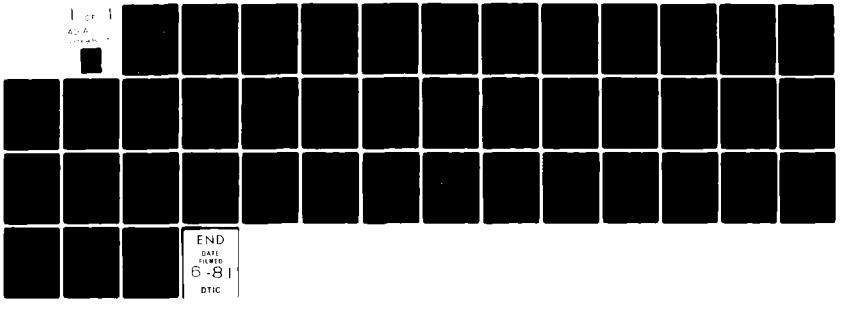

END
DATE FILMED
6-81
DTIC

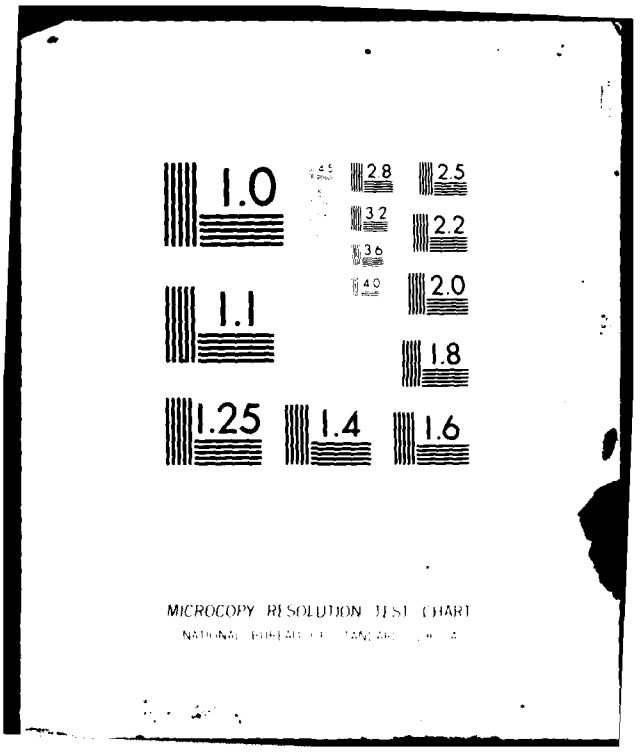
1.0
2.8
2.5
3.2
2.2
3.6
4.0
2.0
1.1
1.8
1.25
1.4
1.6
MICROCOPY RESOLUTION TEST CHART

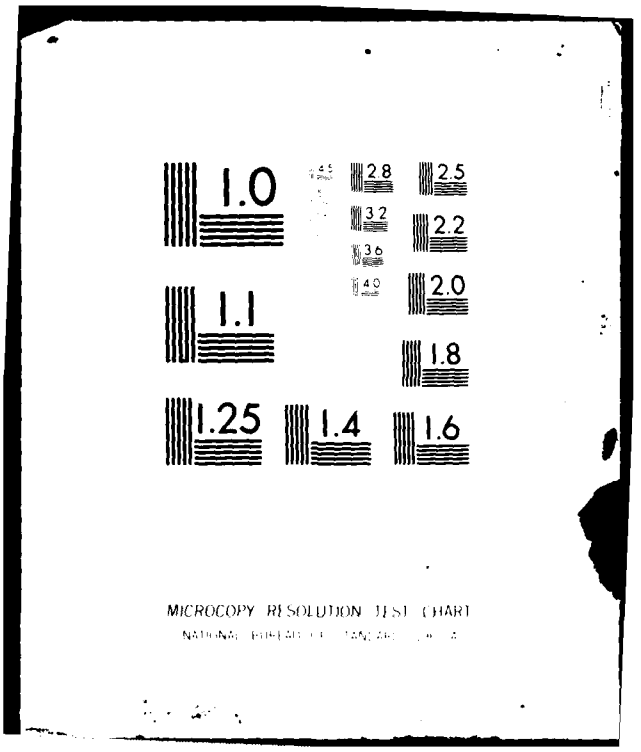
1.0
2.8
2.5
3.2
2.2
3.6
4.0
2.0
1.1
1.8
1.25
1.4
1.6
MICROCOPY RESOLUTION TEST CHART

AD A099517

LEVEL II

(12)

SC

(14) PE-
Report No. 28935

GROWTH OF ALUMINUM GALLIUM NITRIDE FILMS FOR ELECTRO-OPTIC DEVICE APPLICATIONS.

(10) Donald L. Smith [redacted] Richard H. Bruce
Perkin-Elmer Corporation, M.S. 283
Main Avenue, Norwalk, Connecticut 06856

DTIC
ELECTE
JUN 0 1 1981
S E

(11) 15 Feb [redacted] 81

(12) 44

(9) Final Report. 6 Sep [redacted] 77-15 Feb [redacted] 81,

Approved for public release; distribution unlimited.
Reproduction in whole or in part is permitted for any purposes of the United States Government.

(15) N00014-77-C-0492

Prepared for:
Physical Sciences Division
Office of Naval Research
800 N. Quincy Street
Arlington, Va. 22217

DTIC FILE COPY

279550

Contract No. #N00014-77-C-0492

81 6 01 174

AD A099517

LEVEL II

(12)

SC

(14) PE-
Report No. 28935

GROWTH OF ALUMINUM GALLIUM NITRIDE FILMS FOR ELECTRO-OPTIC DEVICE APPLICATIONS.

(10) Donald L. Smith [redacted] Richard H. Bruce
Perkin-Elmer Corporation, M.S. 283
Main Avenue, Norwalk, Connecticut 06856

DTIC
ELECTE
JUN 0 1 1981
S E

(11) 15 Feb [redacted] 81

(12) 44

(9) Final Report. 6 Sep [redacted] 77-15 Feb [redacted] 81,

Approved for public release; distribution unlimited.
Reproduction in whole or in part is permitted for any purposes of the United States Government.

(15) N00014-77-C-0492

Prepared for:
Physical Sciences Division
Office of Naval Research
800 N. Quincy Street
Arlington, Va. 22217

DTIC FILE COPY

279550

Contract No. #N00014-77-C-0492

81 6 01 174

SECURITY CLASSIFICATION OF THIS PAGE (When Data Entered)

REPORT DOCUMENTATION PAGE	READ INSTRUCTIONS BEFORE COMPLETING FORM
1. REPORT NUMBER 28935 / 2. GOVT ACCESSION NO. AD-A099 517	3. RECIPIENT'S CATALOG NUMBER
4. TITLE (and Subtitle) Growth of Aluminum Gallium Nitride Thin Films for Electro-optic Device Applications	5. TYPE OF REPORT & PERIOD COVERED Final Report Sept. 6, 1977 - Feb, 15, 1981
	6. PERFORMING ORG. REPORT NUMBER
7. AUTHOR(s) Donald L. Smith and Richard H. Bruce	8. CONTRACT OR GRANT NUMBER(s) N00014-77-C-0492
9. PERFORMING ORGANIZATION NAME AND ADDRESS Perkin-Elmer Corporation, M.S. 283 Main Avenue, Norwalk, Conn. 06856	10. PROGRAM ELEMENT, PROJECT, TASK AREA & WORK UNIT NUMBERS
11. CONTROLLING OFFICE NAME AND ADDRESS Physical Sciences Div., ONR 800N Quincy St., Arlington, VA 22217	12. REPORT DATE Feb. 15, 1981
	13. NUMBER OF PAGES 40
14. MONITORING AGENCY NAME & ADDRESS(if different from Controlling Office)	15. SECURITY CLASS. (of this report) Unclassified
	15a. DECLASSIFICATION/DOWNGRADING SCHEDULE

16. DISTRIBUTION STATEMENT (of this Report)

Approved for public release; distribution unlimited.

17. DISTRIBUTION STATEMENT (of the abstract entered in Block 20, if different from Report)

18. SUPPLEMENTARY NOTES

19. KEY WORDS (Continue on reverse side if necessary and identify by block number)

gallium nitride, reactive sputtering, epitaxy, photoemission, doping, self-compensation, resistivity

20. ABSTRACT (Continue on reverse side if necessary and identify by block number)

Highly p-doped (AlGa)N offers the prospect of very efficient and sharp-cutoff solar-blind photocathodes, as well as near-UV solid-state lasers. However, AlN reported to date has been semi-insulating, and GaN has been semi-insulating or n-type. Spontaneous generation of compensating N-vacancy donors is believed responsible for the inability to p-dope GaN. In this work, GaN was deposited on sapphire by reaction of Ga with a high-pressure (100 Pa) N_2 plasma over the substrate. High plasma pressure and

DD FORM 1 JAN 73 1473 EDITION OF 1 NOV 65 IS OBSOLETE

S/N 0102-LF-014-6601

SECURITY CLASSIFICATION OF THIS PAGE (When Data Entered)

SECURITY CLASSIFICATION OF THIS PAGE (When Data Entered)

REPORT DOCUMENTATION PAGE	READ INSTRUCTIONS BEFORE COMPLETING FORM
1. REPORT NUMBER 28935 / 2. GOVT ACCESSION NO. AD-A099 517	3. RECIPIENT'S CATALOG NUMBER
4. TITLE (and Subtitle) Growth of Aluminum Gallium Nitride Thin Films for Electro-optic Device Applications	5. TYPE OF REPORT & PERIOD COVERED Final Report Sept. 6, 1977 - Feb, 15, 1981
	6. PERFORMING ORG. REPORT NUMBER
7. AUTHOR(s) Donald L. Smith and Richard H. Bruce	8. CONTRACT OR GRANT NUMBER(s) N00014-77-C-0492
9. PERFORMING ORGANIZATION NAME AND ADDRESS Perkin-Elmer Corporation, M.S. 283 Main Avenue, Norwalk, Conn. 06856	10. PROGRAM ELEMENT, PROJECT, TASK AREA & WORK UNIT NUMBERS
11. CONTROLLING OFFICE NAME AND ADDRESS Physical Sciences Div., ONR 800N Quincy St., Arlington, VA 22217	12. REPORT DATE Feb. 15, 1981
	13. NUMBER OF PAGES 40
14. MONITORING AGENCY NAME & ADDRESS(if different from Controlling Office)	15. SECURITY CLASS. (of this report) Unclassified
	15a. DECLASSIFICATION/DOWNGRADING SCHEDULE

16. DISTRIBUTION STATEMENT (of this Report)

Approved for public release; distribution unlimited.

17. DISTRIBUTION STATEMENT (of the abstract entered in Block 20, if different from Report)

18. SUPPLEMENTARY NOTES

19. KEY WORDS (Continue on reverse side if necessary and identify by block number)

gallium nitride, reactive sputtering, epitaxy, photoemission, doping, self-compensation, resistivity

20. ABSTRACT (Continue on reverse side if necessary and identify by block number)

Highly p-doped (AlGa)N offers the prospect of very efficient and sharp-cutoff solar-blind photocathodes, as well as near-UV solid-state lasers. However, AlN reported to date has been semi-insulating, and GaN has been semi-insulating or n-type. Spontaneous generation of compensating N-vacancy donors is believed responsible for the inability to p-dope GaN. In this work, GaN was deposited on sapphire by reaction of Ga with a high-pressure (100 Pa) N_2 plasma over the substrate. High plasma pressure and

DD FORM 1 JAN 73 1473 EDITION OF 1 NOV 65 IS OBSOLETE

S/N 0102-LF-014-6601

SECURITY CLASSIFICATION OF THIS PAGE (When Data Entered)

low substrate temperature were used in order to inhibit N-vacancy formation. Be, a likely and low-volatility p-dopant, was co-deposited.

After it proved impractical to introduce Ga into the N_2 plasma by evaporation, it was sputtered in a 100 Pa DC N_2 plasma with much better success. Epitaxy of undoped films was obtained at 700°C, although films doped to 4-6x10^{20} Be/cm^3 were polycrystalline. All films turned out n-type by thermoelectric probing and exhibited a large activation energy for conduction, indicating the dominance of unintentional deep impurities. Undoped films had resistivities of 4x10^5 ohm-cm at 300°C and 2x10^4 ohm-cm at 600°C. Be doping increased conductivity by X100 and appeared to be acting as deep donor. A cleaner sputtering environment and closer Be control are recommended in the further pursuit of p-type GaN.

low substrate temperature were used in order to inhibit N-vacancy formation. Be, a likely and low-volatility p-dopant, was co-deposited.

After it proved impractical to introduce Ga into the N_2 plasma by evaporation, it was sputtered in a 100 Pa DC N_2 plasma with much better success. Epitaxy of undoped films was obtained at 700°C, although films doped to 4-6x10^{20} Be/cm^3 were polycrystalline. All films turned out n-type by thermoelectric probing and exhibited a large activation energy for conduction, indicating the dominance of unintentional deep impurities. Undoped films had resistivities of 4x10^5 ohm-cm at 300°C and 2x10^4 ohm-cm at 600°C. Be doping increased conductivity by X100 and appeared to be acting as deep donor. A cleaner sputtering environment and closer Be control are recommended in the further pursuit of p-type GaN.

SUMMARY

Highly p-doped (AlGa)N offers the prospect of very efficient and sharp-cutoff solar-blind photocathodes, as well as near-UV solid-state lasers. However, AlN reported to date has been semi-insulating, and GaN has been semi-insulating or n-type. Spontaneous generation of compensating N-vacancy donors is believed responsible for the inability to p-dope GaN. In this work, GaN was deposited on sapphire by reaction of Ga with a high-pressure (100 Pa) N_2^+ plasma over the substrate. High plasma pressure and low substrate temperature were used in order to inhibit N-vacancy formation. Be, a likely and low-volatility p-dopant, was co-deposited.

After it proved impractical to introduce Ga into the N_2^+ plasma by evaporation, it was sputtered in a 100 Pa DC N_2^+ plasma with much better success. Epitaxy of undoped films was obtained at 700°C, although films doped to 4-6x10^{20} Be/cm^3 were polycrystalline. All films turned out n-type by thermoelectric probing and exhibited a large activation energy for conduction, indicating the dominance of unintentional deep impurities. Undoped films had resistivities of 4x10^5 ohm-cm at 300°C and 2x10^4 ohm-cm at 600°C. Be doping increased conductivity by X100 and appeared to be acting as a deep donor. A cleaner sputtering environment and closer Be control are recommended in the further pursuit of p-type GaN.

Accession For
NTIS GRA&I
DTIC TAB
Unannounced
Justification
By
Distribution/
Availability Codes
Dist | Avail and/or Special
A

ACKNOWLEDGEMENTS

Most of the experiments reported herein were carried out by Paul Saviano; technical assistance was also provided by David Dietrick. Jacques Pankove provided photoluminescence measurements, and the suggestion to use sputtering was provided by Alan Reinberg. Helpful discussions were held with Rointan Bunshah, Maurice Francombe, James Van Vechten, and David Yaney.

ACKNOWLEDGEMENTS

Most of the experiments reported herein were carried out by Paul Saviano; technical assistance was also provided by David Dietrick. Jacques Pankove provided photoluminescence measurements, and the suggestion to use sputtering was provided by Alan Reinberg. Helpful discussions were held with Rointan Bunshah, Maurice Francombe, James Van Vechten, and David Yaney.

TABLE OF CONTENTS

		PAGE
I.	INTRODUCTION	
	A. Objective	1
	B. GaN Conductivity	2
	C. Previous GaN Growth Work	4
	1. Chemical Vapor Deposition (CVD)	4
	2. Reactive Sputtering	4
	3. Reactive Evaporation	5
II.	EXPERIMENTAL APPROACH	
	A. Reactive Evaporation	6
	B. Reactive DC Sputtering	7
	C. Electrical Measurements	9
III.	RESULTS	
	A. Growth Behavior	11
	B. Optical Properties	13
	C. Electrical Measurements	13
IV.	CONCLUSIONS	
	REFERENCES	19
	APPENDIX A: Negative Electron Affinity Photoemission	21
	References	26
	APPENDIX B: Reactive Evaporator Design	27
	DISTRIBUTION LIST	33

TABLE OF CONTENTS

		PAGE
I.	INTRODUCTION	
	A. Objective	1
	B. GaN Conductivity	2
	C. Previous GaN Growth Work	4
	1. Chemical Vapor Deposition (CVD)	4
	2. Reactive Sputtering	4
	3. Reactive Evaporation	5
II.	EXPERIMENTAL APPROACH	
	A. Reactive Evaporation	6
	B. Reactive DC Sputtering	7
	C. Electrical Measurements	9
III.	RESULTS	
	A. Growth Behavior	11
	B. Optical Properties	13
	C. Electrical Measurements	13
IV.	CONCLUSIONS	
	REFERENCES	19
	APPENDIX A: Negative Electron Affinity Photoemission	21
	References	26
	APPENDIX B: Reactive Evaporator Design	27
	DISTRIBUTION LIST	33

I. INTRODUCTION

A. Objective

AlN and GaN are semiconductors with large direct bandgaps corresponding to photon energies in the near UV and therefore have potential for a variety of electro-optic devices operating in this spectral range. Use of the solid solution $Al_xGa_{1-x}N$ would provide device wavelength flexibility from 0.20 to 0.34 μm. Doped to highly p-type conductivity and given a low work function coating, (AlGa)N would be expected to exhibit negative electron affinity (NEA) and to therefore behave as a very efficient photocathode with a sharp long-wavelength cutoff at the bandgap photon energy.[1,2] The NEA principle has been dramatically demonstrated for GaAs[3], and is discussed in more detail in Appendix A, specifically with regard to its application to (AlGa)N photocathodes for solar-blind detection. Assuming a linear dependence of bandgap on the Al fraction, $Al_{0.24}Ga_{0.76}N$ would have a cutoff at 0.29 μm, optimum for solar-blind detector application. (AlGa)N solutions have in fact exhibited a shift in the near-gap photoluminescence band toward shorter wavelength with increasing x.[4,5]

The central problem in achieving such a device is obtaining high p-type conductivity. AlN is generally insulating, and although p-type conductivity has been reported,[6,7] material was high resistivity and consequently of very low carrier concentration. GaN is generally n-type, and most attempts at p-doping have resulted in semi-insulating material, as discussed in Section C.

This report concentrates on attempts to grow p-type GaN thin films by establishing growth conditions which we had reason to believe would maximize the probability of achieving that result. Original plans also

I. INTRODUCTION

A. Objective

AlN and GaN are semiconductors with large direct bandgaps corresponding to photon energies in the near UV and therefore have potential for a variety of electro-optic devices operating in this spectral range. Use of the solid solution $Al_xGa_{1-x}N$ would provide device wavelength flexibility from 0.20 to 0.34 μm. Doped to highly p-type conductivity and given a low work function coating, (AlGa)N would be expected to exhibit negative electron affinity (NEA) and to therefore behave as a very efficient photocathode with a sharp long-wavelength cutoff at the bandgap photon energy.[1,2] The NEA principle has been dramatically demonstrated for GaAs[3], and is discussed in more detail in Appendix A, specifically with regard to its application to (AlGa)N photocathodes for solar-blind detection. Assuming a linear dependence of bandgap on the Al fraction, $Al_{0.24}Ga_{0.76}N$ would have a cutoff at 0.29 μm, optimum for solar-blind detector application. (AlGa)N solutions have in fact exhibited a shift in the near-gap photoluminescence band toward shorter wavelength with increasing x.[4,5]

The central problem in achieving such a device is obtaining high p-type conductivity. AlN is generally insulating, and although p-type conductivity has been reported,[6,7] material was high resistivity and consequently of very low carrier concentration. GaN is generally n-type, and most attempts at p-doping have resulted in semi-insulating material, as discussed in Section C.

This report concentrates on attempts to grow p-type GaN thin films by establishing growth conditions which we had reason to believe would maximize the probability of achieving that result. Original plans also

called for growing (AlGa)N, but is seemed advisable to understand the growth of the simpler binary compound first, and, as it turned out, time did not permit studying the growth of (AlGa)N. GaN was chosen over AlN for study because a solar-blind material would be mostly GaN and because the chances of making material conductive enough to permit electrical measurements were deemed higher for the smaller bandgap material.

Section B discusses the self-compensation phenomenon which is believed to be the source of the difficulty in p-doping GaN and explains our choice of experimental approach in attempting to overcome this problem. Section C reviews previous GaN growth techniques and results.

B. GaN Conductivity

There is considerable evidence that nitrogen vacancies (V_N) are responsible for the n-type conductivity observed in GaN. A V_N is expected to act as a donor[8], because the N which would have held the bond electron donated from neighboring Ga is missing, and the electron goes instead into the conduction band. By analogy, V_{As} has been shown to be a donor in GaAs[9]. The antisite defect N_{Ga}, which would also be a donor, is calculated to have a much higher energy of formation than V_N[9]. N-poor material would indeed be expected based on the very high equilibrium vapor pressure calculated for N_2 over GaN at the usual growth temperatures (10^2 atm. at 1000°C)[10].

The failure to be able to p-dope GaN may be due to self-compensation, a phenomenon common to high-bandgap semiconductors which involves compensation of impurity dopants by the spontaneous generation of native point defects of the opposite carrier type. In GaN,

$$N_N \longrightarrow V_N^+ + N_i + n \qquad (1)$$

is the likely mechanism. The interstitial nitrogen, N_i, so generated, may remain in solid solution, generate N_{Ga}, or migrate to dislocations, grain boundaries, or to the surface. Reaction (1) will proceed if the

called for growing (AlGa)N, but is seemed advisable to understand the growth of the simpler binary compound first, and, as it turned out, time did not permit studying the growth of (AlGa)N. GaN was chosen over AlN for study because a solar-blind material would be mostly GaN and because the chances of making material conductive enough to permit electrical measurements were deemed higher for the smaller bandgap material.

Section B discusses the self-compensation phenomenon which is believed to be the source of the difficulty in p-doping GaN and explains our choice of experimental approach in attempting to overcome this problem. Section C reviews previous GaN growth techniques and results.

B. GaN Conductivity

There is considerable evidence that nitrogen vacancies (V_N) are responsible for the n-type conductivity observed in GaN. A V_N is expected to act as a donor[8], because the N which would have held the bond electron donated from neighboring Ga is missing, and the electron goes instead into the conduction band. By analogy, V_{As} has been shown to be a donor in GaAs[9]. The antisite defect N_{Ga}, which would also be a donor, is calculated to have a much higher energy of formation than V_N[9]. N-poor material would indeed be expected based on the very high equilibrium vapor pressure calculated for N_2 over GaN at the usual growth temperatures (10^2 atm. at 1000°C)[10].

The failure to be able to p-dope GaN may be due to self-compensation, a phenomenon common to high-bandgap semiconductors which involves compensation of impurity dopants by the spontaneous generation of native point defects of the opposite carrier type. In GaN,

$$N_N \longrightarrow V_N^+ + N_i + n \qquad (1)$$

is the likely mechanism. The interstitial nitrogen, N_i, so generated, may remain in solid solution, generate N_{Ga}, or migrate to dislocations, grain boundaries, or to the surface. Reaction (1) will proceed if the

heat of reaction required is less than that supplied by recombination of the electron generated with the hole from the impurity acceptor. The latter energy is the bandgap energy, so the process becomes more likely for high-bandgap materials. Recombination of the holes with the electrons from reaction (1) renders the material semi-insulating. Thermodynamic calculations predict that, at equilibrium, self-compensation will be complete for GaN and AlN[11]. It has also been suggested recently that compensation can be caused by the activation of amphoteric impurities[12] as well as of native point defects such as V_N.

The present work attempted to overcome the above difficulties in three ways:

1. An N_2 plasma was maintained over the growth surface under conditions believed to maximize the concentration of active nitrogen species (N_2*, N*, and N). It was reasoned that this, in turn, would maximize the coverage of adsorbed N atoms on the growth surface and thus drive reaction (1) in the reverse direction.

2. Substrate temperature was held at the minimum consistent with acceptable crystal quality so as to "freeze" reaction (1), that is, prevent it from receiving the activation energy needed in order for it to proceed towards equilibrium.

3. An impurity dopant (Be) was selected which is expected to behave primarily as an acceptor, as do all of the Group II elements on Group III sites in the III-V semiconductors. Be has the lowest vapor pressure of all the Group II elements, thus maximizing incorporation efficiency. Although Group IA and IIA elements can also act as donors, when in interstitial sites, substitutional site solubility is generally much higher than interstitial solubility.

heat of reaction required is less than that supplied by recombination of the electron generated with the hole from the impurity acceptor. The latter energy is the bandgap energy, so the process becomes more likely for high-bandgap materials. Recombination of the holes with the electrons from reaction (1) renders the material semi-insulating. Thermodynamic calculations predict that, at equilibrium, self-compensation will be complete for GaN and AlN[11]. It has also been suggested recently that compensation can be caused by the activation of amphoteric impurities[12] as well as of native point defects such as V_N.

The present work attempted to overcome the above difficulties in three ways:

1. An N_2 plasma was maintained over the growth surface under conditions believed to maximize the concentration of active nitrogen species (N_2*, N*, and N). It was reasoned that this, in turn, would maximize the coverage of adsorbed N atoms on the growth surface and thus drive reaction (1) in the reverse direction.

2. Substrate temperature was held at the minimum consistent with acceptable crystal quality so as to "freeze" reaction (1), that is, prevent it from receiving the activation energy needed in order for it to proceed towards equilibrium.

3. An impurity dopant (Be) was selected which is expected to behave primarily as an acceptor, as do all of the Group II elements on Group III sites in the III-V semiconductors. Be has the lowest vapor pressure of all the Group II elements, thus maximizing incorporation efficiency. Although Group IA and IIA elements can also act as donors, when in interstitial sites, substitutional site solubility is generally much higher than interstitial solubility.

C. Previous GaN Growth Work

1. Chemical Vapor Deposition (CVD)

Most GaN has been grown by CVD, using as reactant gases NH_3 and N_2 with either metal chlorides (GaCl)[13-18] or metal-organics ($Ga(CH_3)_3$).[19,20] Minimum temperature for epitaxy on sapphire has been 825°C[13] in growth from the chlorides. In cases where RF-plasma activation of the CVD reaction has been employed,[17,20] the epitaxial temperature has been reduced to 600°C. The reduction of epitaxial temperature by plasma activation is a commonly observed phenomenon.[21]

Unintentionally-doped GaN almost always exhibits high n-type conductivity with carrier concentrations around 10^{19} n/cm^3, although $<10^{17} n/cm^3$ has been observed.[15] The carriers have been attributed to N-vacancies[13] which in extreme cases also impart a green color to the films. The n-type carriers can be compensated out by the addition of p-type dopants, leaving the material semi-insulating. This effect has been demonstrated using Li[18], Zn[13], and Mg[13]. The amphoteric dopants Si and Ge have also been employed.[13] These materials act as donors in III-sites and acceptors in V-sites. Si reduced carrier concentration in CVD GaN to $3x10^{16}$ n/cm^3, and Ge converted it to $6x10^{18}$ P/cm^3, but the latter material was inhomogeneous and difficult to reproduce. One group which reported p-type conductivity in GaN[22] later termed the material "nearly insulating but with p-tendency".[23] Plasma-activated CVD was shown to produce semi-insulating GaN without the use of external compensating dopants.[20] This result suggests a higher-than-usual degree of stoichiometry which may be attributable to the much lower substrate temperature employed in that work and to the resulting decrease in the rate of N loss, although it is also possible that a very low mobility was responsible for the high resistivity.

2. Reactive Sputtering

Reactive sputtering has been used to grow GaN,[24,25] using a N_2 discharge to erode a Ga-covered target. No epitaxy was observed although

C. Previous GaN Growth Work

1. Chemical Vapor Deposition (CVD)

Most GaN has been grown by CVD, using as reactant gases NH_3 and N_2 with either metal chlorides (GaCl)[13-18] or metal-organics ($Ga(CH_3)_3$).[19,20] Minimum temperature for epitaxy on sapphire has been 825°C[13] in growth from the chlorides. In cases where RF-plasma activation of the CVD reaction has been employed,[17,20] the epitaxial temperature has been reduced to 600°C. The reduction of epitaxial temperature by plasma activation is a commonly observed phenomenon.[21]

Unintentionally-doped GaN almost always exhibits high n-type conductivity with carrier concentrations around 10^{19} n/cm^3, although $<10^{17} n/cm^3$ has been observed.[15] The carriers have been attributed to N-vacancies[13] which in extreme cases also impart a green color to the films. The n-type carriers can be compensated out by the addition of p-type dopants, leaving the material semi-insulating. This effect has been demonstrated using Li[18], Zn[13], and Mg[13]. The amphoteric dopants Si and Ge have also been employed.[13] These materials act as donors in III-sites and acceptors in V-sites. Si reduced carrier concentration in CVD GaN to $3x10^{16}$ n/cm^3, and Ge converted it to $6x10^{18}$ P/cm^3, but the latter material was inhomogeneous and difficult to reproduce. One group which reported p-type conductivity in GaN[22] later termed the material "nearly insulating but with p-tendency".[23] Plasma-activated CVD was shown to produce semi-insulating GaN without the use of external compensating dopants.[20] This result suggests a higher-than-usual degree of stoichiometry which may be attributable to the much lower substrate temperature employed in that work and to the resulting decrease in the rate of N loss, although it is also possible that a very low mobility was responsible for the high resistivity.

2. Reactive Sputtering

Reactive sputtering has been used to grow GaN,[24,25] using a N_2 discharge to erode a Ga-covered target. No epitaxy was observed although

a preferred crystal orientation was reported. A study of crystal properties indicated that the GaN became more stoichiometic as the ambient pressure increased.[25] Depositions at pressures as high as 3 Pa were accomplished, but no definitive electrical measurements were made, and no doping was attempted.

3. Reactive Evaporation

GaN has also been grown by reactive evaporation.[26,27] Both studies were done in a high vacuum environment ($<10^{-3}$ Pa). Active nitrogen generated in a microwave discharge effused from an orifice in the discharge chamber into the vacuum and was directed at the heated substrate along with a beam of thermally-evaporated Ga. A maximum brightness in the afterglow of the plasma was observed at N_2 pressures around 400 Pa.[27] Epitaxy was achieved at substrate temperatures greater than 550°C,[26] but no electrical measurements were made on these films.

Plots of log(P) vs. 1/°K for polycrystalline films grown at substrate temperatures between 200 and 400°C showed linear relationships between 100 and 300°C, and slopes were used to calculate activation energy for conduction.[27] Results were as shown in Table I. N-type mobilities were marginally detectable at 300°C with a detection limit of 5 cm^2/V-sec.

TABLE I. Electrical Properties of Reactively-Evaporated GaN[27]

substrate temp., °C	ρ at 600°C ohm-cm	activation energy, eV
200	7300	0.86
300	200	0.47
400	48	0.34

a preferred crystal orientation was reported. A study of crystal properties indicated that the GaN became more stoichiometic as the ambient pressure increased.[25] Depositions at pressures as high as 3 Pa were accomplished, but no definitive electrical measurements were made, and no doping was attempted.

3. Reactive Evaporation

GaN has also been grown by reactive evaporation.[26,27] Both studies were done in a high vacuum environment ($<10^{-3}$ Pa). Active nitrogen generated in a microwave discharge effused from an orifice in the discharge chamber into the vacuum and was directed at the heated substrate along with a beam of thermally-evaporated Ga. A maximum brightness in the afterglow of the plasma was observed at N_2 pressures around 400 Pa.[27] Epitaxy was achieved at substrate temperatures greater than 550°C,[26] but no electrical measurements were made on these films.

Plots of log(P) vs. 1/°K for polycrystalline films grown at substrate temperatures between 200 and 400°C showed linear relationships between 100 and 300°C, and slopes were used to calculate activation energy for conduction.[27] Results were as shown in Table I. N-type mobilities were marginally detectable at 300°C with a detection limit of 5 cm^2/V-sec.

TABLE I. Electrical Properties of Reactively-Evaporated GaN[27]

substrate temp., °C	ρ at 600°C ohm-cm	activation energy, eV
200	7300	0.86
300	200	0.47
400	48	0.34

II. EXPERIMENTAL APPROACH

A. Reactive Evaporation

To realize the desirable growth conditions outlined in Section IB, a system was constructed to evaporate Ga into an intense N_2 plasma maintained directly over the wafer. The system was designed to operate at pressures around 100-400 Pa, where maximum N atom production has been observed.[27-29] This is about $x10^2$ higher N_2 pressure over the substrate than is typical in sputter deposition such as the work discussed in Section IC2, and about $x10^5$ higher than the N_2 beam pressure during the reactive evaporation of Section IC3. The Ga has a small mean free path at these pressures and consequently must be carried to the substrate by diffusion and the N_2 flow stream. Details of the development of this apparatus are provided in Appendix B.

The substrate material was sapphire (1000), chosen because of previous successful epitaxy (Section IC1) and because its high resistivity permits film electrical measurements. Wafers were chemically polished commercially (Insaco Corp.), swabbed with dilute detergent (Orion), rinsed in deionized water, and blown dry with filtered dry N_2. This procedure resulted in a surface which gave low-energy electron diffraction (LEED) patterns having sharp beams and low diffuse background at 199 eV without further cleaning under vacuum. In addition, substrates were heated to 600°C briefly just prior to growth to desorb residual surface contamination.

Many different growth conditions were investigated, but all gave unsatisfactory results, with the main problem being irreproducibility. The growth parameters studied included Ga source temperature, N_2 flow rate, pressure and RF power. Depositions at substrate temperatures above room temperature were not attempted, since even at room temperature results were not controllable. The temperature of the Ga source was varied around 1000°C, which corresponded to a calculated deposition rate of about 100 Å/min. The pressure was varied from 50 to 150 Pa with most work done near 70 Pa. The N_2 flow was varied from 0 to 400 sccm with most work done at 200 sccm. The RF power was varied from about 0.25 W/cm^3 to 13 W/cm^3.

II. EXPERIMENTAL APPROACH

A. Reactive Evaporation

To realize the desirable growth conditions outlined in Section IB, a system was constructed to evaporate Ga into an intense N_2 plasma maintained directly over the wafer. The system was designed to operate at pressures around 100-400 Pa, where maximum N atom production has been observed.[27-29] This is about $x10^2$ higher N_2 pressure over the substrate than is typical in sputter deposition such as the work discussed in Section IC2, and about $x10^5$ higher than the N_2 beam pressure during the reactive evaporation of Section IC3. The Ga has a small mean free path at these pressures and consequently must be carried to the substrate by diffusion and the N_2 flow stream. Details of the development of this apparatus are provided in Appendix B.

The substrate material was sapphire (1000), chosen because of previous successful epitaxy (Section IC1) and because its high resistivity permits film electrical measurements. Wafers were chemically polished commercially (Insaco Corp.), swabbed with dilute detergent (Orion), rinsed in deionized water, and blown dry with filtered dry N_2. This procedure resulted in a surface which gave low-energy electron diffraction (LEED) patterns having sharp beams and low diffuse background at 199 eV without further cleaning under vacuum. In addition, substrates were heated to 600°C briefly just prior to growth to desorb residual surface contamination.

Many different growth conditions were investigated, but all gave unsatisfactory results, with the main problem being irreproducibility. The growth parameters studied included Ga source temperature, N_2 flow rate, pressure and RF power. Depositions at substrate temperatures above room temperature were not attempted, since even at room temperature results were not controllable. The temperature of the Ga source was varied around 1000°C, which corresponded to a calculated deposition rate of about 100 Å/min. The pressure was varied from 50 to 150 Pa with most work done near 70 Pa. The N_2 flow was varied from 0 to 400 sccm with most work done at 200 sccm. The RF power was varied from about 0.25 W/cm^3 to 13 W/cm^3.

Besides irreproducibility of deposition, other difficulties encountered were low rates when deposition did occur and black particulate matter in the film. The most likely cause of the irreproducibility is activated nitrogen reacting with the Ga source. A thin crust was observed to form on the Ga surface after operation of a plasma. This crust was probably GaN and could have hindered subsequent evaporation. The particulate matter was probably due to gas phase agglomeration of diffusing Ga atoms into droplets which then partially reacted to GaN as they traversed the plasma.

Because of these difficulties, this approach was abandoned towards the end of the program, and a preliminary and much more successful attempt was made at an alternative approach to achieving the objectives outlined in Section IB. This work is described in Section B below, and all film analysis results reported in Section III relate to GaN grown by this latter approach.

B. Reactive DC Sputtering

Sputtering is a method which allows introduction of Ga into an N_2 plasma in spite of a strong Ga surface reaction, because the surface nitride thus formed is being continuously sputtered away. Though sputtering is most efficient at pressures around 1 Pa, we have demonstrated here that it is possible to achieve deposition at much higher pressures if the target is located very close to the substrate. The growth chamber used for reactive evaporation was modified to achieve high pressure sputtering (Fig. 1). Other details of the growth system are the same as described in Appendix B. The substrate, at ground potential, was held to a temperature controlled Mo platform by W wire clips. A layer of Ga between the substrate and the Mo was used to improve thermal contact, but it often reacted away during the course of a growth run. The target electrode, at -800VDC, was composed of a stainless steel rod surrounded by a ceramic collar to confine the discharge. A layer of 7-nines pure Ga was spread on the electrode end. The DC plasma used could be confined to the vicinity of the gallium layer by the ceramic in-

Besides irreproducibility of deposition, other difficulties encountered were low rates when deposition did occur and black particulate matter in the film. The most likely cause of the irreproducibility is activated nitrogen reacting with the Ga source. A thin crust was observed to form on the Ga surface after operation of a plasma. This crust was probably GaN and could have hindered subsequent evaporation. The particulate matter was probably due to gas phase agglomeration of diffusing Ga atoms into droplets which then partially reacted to GaN as they traversed the plasma.

Because of these difficulties, this approach was abandoned towards the end of the program, and a preliminary and much more successful attempt was made at an alternative approach to achieving the objectives outlined in Section IB. This work is described in Section B below, and all film analysis results reported in Section III relate to GaN grown by this latter approach.

B. Reactive DC Sputtering

Sputtering is a method which allows introduction of Ga into an N_2 plasma in spite of a strong Ga surface reaction, because the surface nitride thus formed is being continuously sputtered away. Though sputtering is most efficient at pressures around 1 Pa, we have demonstrated here that it is possible to achieve deposition at much higher pressures if the target is located very close to the substrate. The growth chamber used for reactive evaporation was modified to achieve high pressure sputtering (Fig. 1). Other details of the growth system are the same as described in Appendix B. The substrate, at ground potential, was held to a temperature controlled Mo platform by W wire clips. A layer of Ga between the substrate and the Mo was used to improve thermal contact, but it often reacted away during the course of a growth run. The target electrode, at -800VDC, was composed of a stainless steel rod surrounded by a ceramic collar to confine the discharge. A layer of 7-nines pure Ga was spread on the electrode end. The DC plasma used could be confined to the vicinity of the gallium layer by the ceramic in-

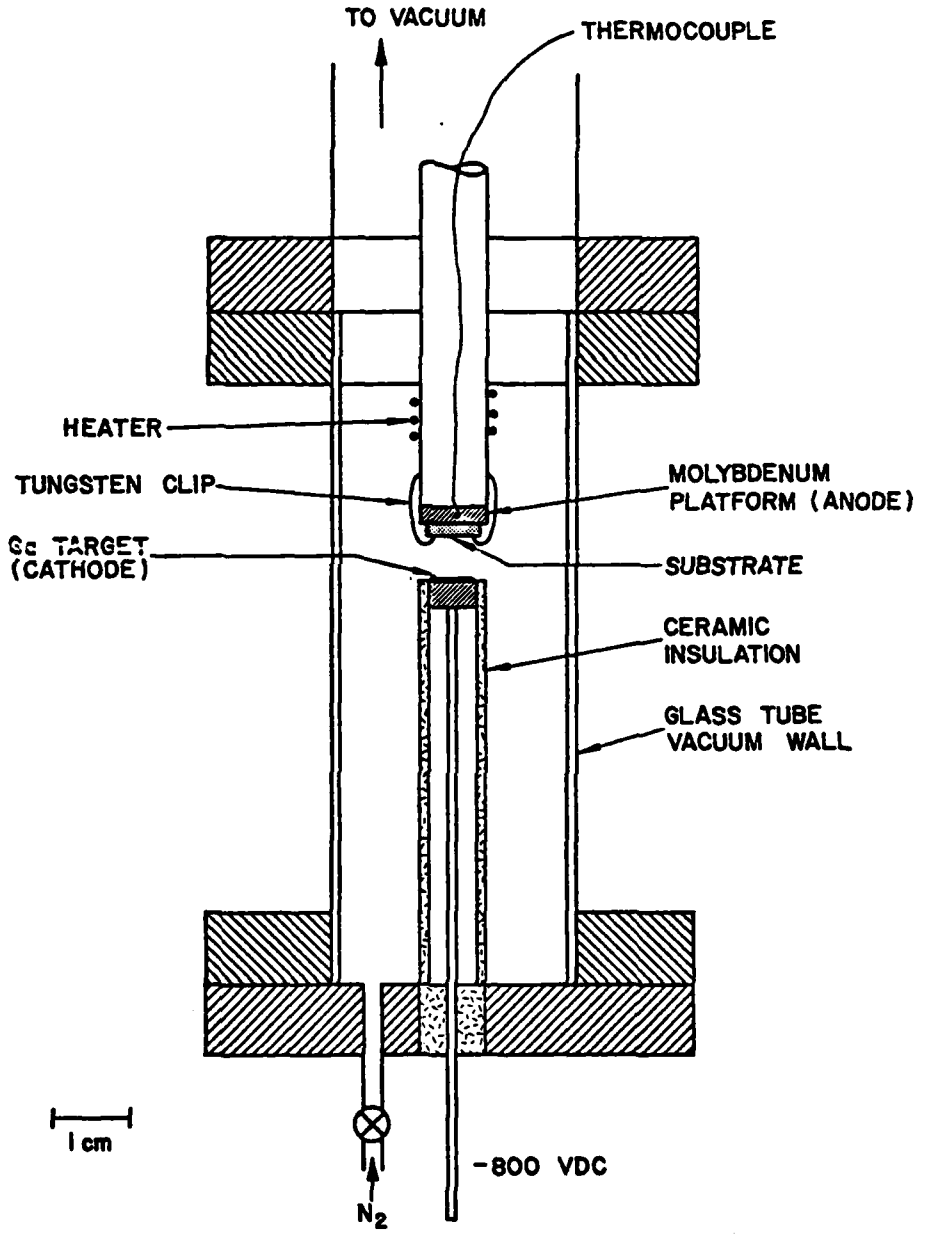

Figure 1. High Pressure DC Sputtering Reactor

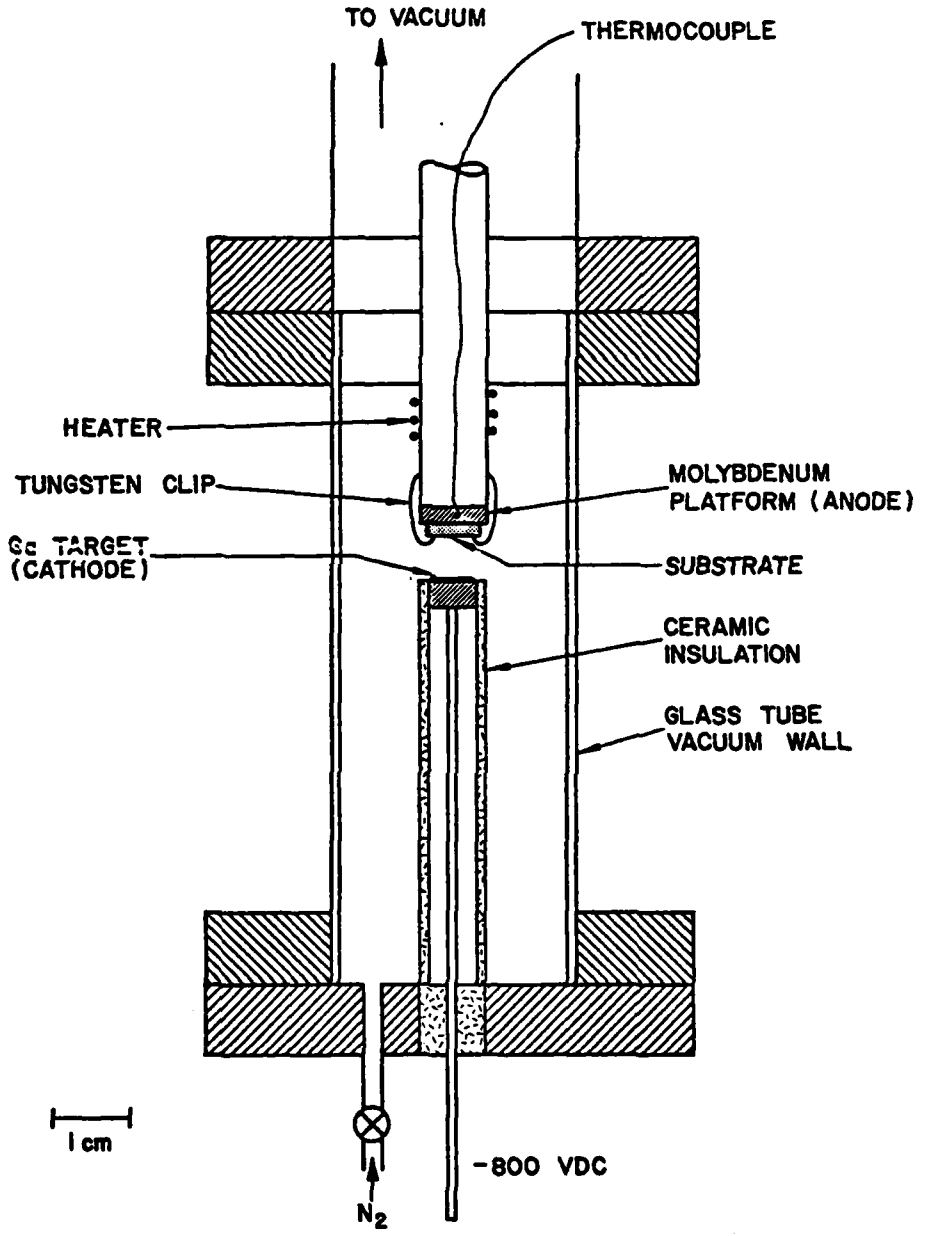

Figure 1. High Pressure DC Sputtering Reactor

sulating collar. The substrate holder served as an anode. The nitrogen was introduced below the cathode and evacuated above the anode. A quartz sleeve was used as an outer wall. The chamber could be evacuated to 10^{-6} Pa by a 50 l/sec ion pump. During operation, liquid nitrogen sorption pumps were used to recieve the nitrogen flow.

The substrate-target spacing was made small (4-12 mm) to maximize deposition at high pressure. The discharge was not confined to the target-substrate vicinity but extended beyond the substrate. This was necessary in order to maintain the discharge over the insulating substrate. This discharge extension did reduce the active nitrogen concentration at the substrate surface and consequently was minimized by flow, power, and pressure adjustments. Most GaN was grown at 133 Pa of N_2 with a 14 sccm flow and about 2 W/cm^2 of plasma power density. Dopants were introduced in different ways. Tin was dissolved in the target Ga to 0.1 atomic percent. Beryllium, however, was found to have a low solubility of around $2x10^{-3}$%, so a flake of it was placed on the Ga surface, covering approximately 0.1% of the target area. Assuming similar sputter rates for Ga and Be, this coverage would dope the GaN to $2x10^{19}$ Be/cm^{-3}. Atomic absorption analysis of Be content indicated that $4\text{-}6x10^{20}$ Be/cm^3 was obtained.

C. Electrical Measurements

Resistivity and Hall voltage were measured using the standard van der Pauw 4-point peripheral contact configuration, in an apparatus allowing measurements up to 600°C in a 10^{-1} Pa ambient. Ga-In liquid eutectic was used for contact from the film to spring-loaded tungsten probes which held the sapphire substrate against a Mo platform. The Mo was heated radiatively by a filament behind it, and its temperature was monitored with a thermocouple spot-welded to it. Two-point resistance measurements were used to monitor contact behavior with temperature and time, and 4-point measurements were made at fixed temperatures under steady-state conditions. Isolation of better than 10^{11} ohms at 600°C between the probes and ground was achieved by using quartz and alumina insulation, by sanding deposits off of the substrate

sulating collar. The substrate holder served as an anode. The nitrogen was introduced below the cathode and evacuated above the anode. A quartz sleeve was used as an outer wall. The chamber could be evacuated to 10^{-6} Pa by a 50 l/sec ion pump. During operation, liquid nitrogen sorption pumps were used to recieve the nitrogen flow.

The substrate-target spacing was made small (4-12 mm) to maximize deposition at high pressure. The discharge was not confined to the target-substrate vicinity but extended beyond the substrate. This was necessary in order to maintain the discharge over the insulating substrate. This discharge extension did reduce the active nitrogen concentration at the substrate surface and consequently was minimized by flow, power, and pressure adjustments. Most GaN was grown at 133 Pa of N_2 with a 14 sccm flow and about 2 W/cm^2 of plasma power density. Dopants were introduced in different ways. Tin was dissolved in the target Ga to 0.1 atomic percent. Beryllium, however, was found to have a low solubility of around $2x10^{-3}$%, so a flake of it was placed on the Ga surface, covering approximately 0.1% of the target area. Assuming similar sputter rates for Ga and Be, this coverage would dope the GaN to $2x10^{19}$ Be/cm^{-3}. Atomic absorption analysis of Be content indicated that $4\text{-}6x10^{20}$ Be/cm^3 was obtained.

C. Electrical Measurements

Resistivity and Hall voltage were measured using the standard van der Pauw 4-point peripheral contact configuration, in an apparatus allowing measurements up to 600°C in a 10^{-1} Pa ambient. Ga-In liquid eutectic was used for contact from the film to spring-loaded tungsten probes which held the sapphire substrate against a Mo platform. The Mo was heated radiatively by a filament behind it, and its temperature was monitored with a thermocouple spot-welded to it. Two-point resistance measurements were used to monitor contact behavior with temperature and time, and 4-point measurements were made at fixed temperatures under steady-state conditions. Isolation of better than 10^{11} ohms at 600°C between the probes and ground was achieved by using quartz and alumina insulation, by sanding deposits off of the substrate

edges, and by inserting a thin sheet of mica between the substrate and the Mo platform. Measurements were made in the DC mode rather than the AC-synchronous mode in order to be able to monitor offset voltages. Good stability of these offsets was achieved by using a single-ended voltmeter at ground potential in conjunction with a floating, battery-powered constant-current source across the other two probes. The voltmeter was a Keithley electrometer with $>10^{12}$ ohm input impedance. Hall voltages were measured at 2500 Gauss.

Carrier type was determined by thermoelectric probing. A large thermal mass at the hot probe proved important for sufficient signal strength: a pencil-tip soldering iron was used. Noise was lower with the hot probe grounded and the cold probe floating. Ga-In contact metallization reduced noise and increased signal. Tests on 10^{17}-$10^{18}/cm^3$ p- and n-GaAs gave signals of + and - 3nA, respectively, at the cold probe. It was necessary to heat some GaN samples to 200-300°C to obtain enough conductivity for signal generation. This was done on a temperature-controlled hotplate in air.

edges, and by inserting a thin sheet of mica between the substrate and the Mo platform. Measurements were made in the DC mode rather than the AC-synchronous mode in order to be able to monitor offset voltages. Good stability of these offsets was achieved by using a single-ended voltmeter at ground potential in conjunction with a floating, battery-powered constant-current source across the other two probes. The voltmeter was a Keithley electrometer with $>10^{12}$ ohm input impedance. Hall voltages were measured at 2500 Gauss.

Carrier type was determined by thermoelectric probing. A large thermal mass at the hot probe proved important for sufficient signal strength: a pencil-tip soldering iron was used. Noise was lower with the hot probe grounded and the cold probe floating. Ga-In contact metallization reduced noise and increased signal. Tests on 10^{17}-$10^{18}/cm^3$ p- and n-GaAs gave signals of + and - 3nA, respectively, at the cold probe. It was necessary to heat some GaN samples to 200-300°C to obtain enough conductivity for signal generation. This was done on a temperature-controlled hotplate in air.

III. RESULTS

A. Growth Behavior

The discussion below relates only to GaN grown by the DC sputtering technique described in Section IIB. Material grown by reactive evaporation was not of sufficient quality or reproducibility to permit measurements of film properties or their correlation with growth conditions, as discussed in Section IIA.

Table II lists properties of sputtered films grown under a variety of conditions. All films listed were grown on sapphire (0001) in an 800 V, 11 mA discharge of 130 Pa N_2 flowing at 14 sccm. Ga-cathode-to-film distance was usually 12 mm; this parameter was not studied in a systematic way. Film deposition rate varied from 0.04 to 0.20 μm/hr under these conditions, as calculated from film thickness (stylus profiler measurement) and growth time.

Unintentionally-doped and Sn-doped films grown at 700°C substrate temperature all showed some degree of crystalline order in LEED analysis except for no. 8261. No. 9301 showed a single hexagonal array of first-order diffraction beams at 57 eV, characteristic of an epitaxial (0001)-oriented film with no surface structure. LEED beams were well-defined, and diffuse background was low, both indicative of good crystalline order. No. 9191 showed, at 143 eV, 2 additional, weaker hexagons rotated 20° and 40° with respect to the primary hexagon, indicative of a mosaic of crystallites all oriented with the (0001) plane parallel to the substrate, but with some rotated about the (0001) axis to angles of 20° and 40° with respect to the dominant orientation. The ring in no. 9171, which appeared at the same diameter as the hexagonal array, indicates a situation similar to 9191 but with random rotation of some crystallites about the (0001) axis.

The one undoped film grown at 500°C did not yield a LEED pattern, nor did the Be-doped films grown at temperatures between 300 and 700°C, indicating random polycrystalline or amorphous character for all of these films.

III. RESULTS

A. Growth Behavior

The discussion below relates only to GaN grown by the DC sputtering technique described in Section IIB. Material grown by reactive evaporation was not of sufficient quality or reproducibility to permit measurements of film properties or their correlation with growth conditions, as discussed in Section IIA.

Table II lists properties of sputtered films grown under a variety of conditions. All films listed were grown on sapphire (0001) in an 800 V, 11 mA discharge of 130 Pa N_2 flowing at 14 sccm. Ga-cathode-to-film distance was usually 12 mm; this parameter was not studied in a systematic way. Film deposition rate varied from 0.04 to 0.20 μm/hr under these conditions, as calculated from film thickness (stylus profiler measurement) and growth time.

Unintentionally-doped and Sn-doped films grown at 700°C substrate temperature all showed some degree of crystalline order in LEED analysis except for no. 8261. No. 9301 showed a single hexagonal array of first-order diffraction beams at 57 eV, characteristic of an epitaxial (0001)-oriented film with no surface structure. LEED beams were well-defined, and diffuse background was low, both indicative of good crystalline order. No. 9191 showed, at 143 eV, 2 additional, weaker hexagons rotated 20° and 40° with respect to the primary hexagon, indicative of a mosaic of crystallites all oriented with the (0001) plane parallel to the substrate, but with some rotated about the (0001) axis to angles of 20° and 40° with respect to the dominant orientation. The ring in no. 9171, which appeared at the same diameter as the hexagonal array, indicates a situation similar to 9191 but with random rotation of some crystallites about the (0001) axis.

The one undoped film grown at 500°C did not yield a LEED pattern, nor did the Be-doped films grown at temperatures between 300 and 700°C, indicating random polycrystalline or amorphous character for all of these films.

TABLE II. Properties of Sputter-Deposited GaN

(sapphire (0001) substrate; 14 sccm N_2 flow at 1 Torr; 800 VDC, 11 mA discharge)

Film No.	Ga To Film Distance mm	Substrate Temp., °C	Film Thickness μm	Average Growth Rate, μm/hr	Dopant	ρ at 600°C, Ω-cm	LEED Pattern
7292	4	40	0.60	1.2	none		
8111	8	500	0.04	0.05	none		none
8261	6	700			none		none
9191	12	700	0.20	0.20	none	23,000	3 hexagons
9301	12	700	0.84	0.14	none	13,000	hexagon
9171	6	700			Sn		hexagon +ring
11252	12	300	0.06	0.04	Be	77	none
11251	12	500	0.10	0.07	Be	69	none
11253	12	700	0.12	0.08	Be	327	none
11181	12	700	0.19	0.13	Be		

TABLE II. Properties of Sputter-Deposited GaN

(sapphire (0001) substrate; 14 sccm N_2 flow at 1 Torr; 800 VDC, 11 mA discharge)

Film No.	Ga To Film Distance mm	Substrate Temp., °C	Film Thickness μm	Average Growth Rate, μm/hr	Dopant	ρ at 600°C, Ω-cm	LEED Pattern
7292	4	40	0.60	1.2	none		
8111	8	500	0.04	0.05	none		none
8261	6	700			none		none
9191	12	700	0.20	0.20	none	23,000	3 hexagons
9301	12	700	0.84	0.14	none	13,000	hexagon
9171	6	700			Sn		hexagon +ring
11252	12	300	0.06	0.04	Be	77	none
11251	12	500	0.10	0.07	Be	69	none
11253	12	700	0.12	0.08	Be	327	none
11181	12	700	0.19	0.13	Be		

Auger spectroscopy of No's. 9191 and 11253 was done using a retarding-field analyzer, for qualitative elemental analysis. It showed N(5 μV) and Ga (1.2 μV) to be dominant, with smaller amounts of C and O which could have arisen from surface contamination. Sputter cleaning was not carried out.

B. Optical Properties

Optical measurements were made to examine crystal composition and quality. First, the optical absorption was measured at room temperature across the bandgap (Fig. 2). The absorption edge was observed to be quite broad as would be expected at room temperature due to phonon-assisted processes. The absorption edge was in the vicinity of 3.35 eV, where the GaN bandgap has been previously reported. [30]

Laser photoluminescence measurements were made on one epitaxial sample (No. 9301), but very little luminescence was observed.[31] This result suggests that nonradiative transitions are being made through a high density of impurities or defects.

C. Electrical Measurements

Contact resistance between the GaIn metallization and the film generally improved by 1-2 orders of magnitude during heating to and annealing at 600°C for periods up to 15 min. in the probe station at 10^{-1} Pa. In the case of the higher-resistivity, undoped films, film resistance was dominant after the anneal, whereas in the case of the lower-resistivity, Be-doped films, contact resistance remained dominant. Both resistances increased rapidly with decreasing temperature, so that all measurements were made at 600°C except for No. 9301.

Table I shows 4-point resistivity measurements at 600°C for two undoped and three Be-doped films. The undoped films average just over two orders of magnitude higher in resistivity than the Be-doped films. The variation in resistivity with growth conditions within each of these two

Auger spectroscopy of No's. 9191 and 11253 was done using a retarding-field analyzer, for qualitative elemental analysis. It showed N(5 μV) and Ga (1.2 μV) to be dominant, with smaller amounts of C and O which could have arisen from surface contamination. Sputter cleaning was not carried out.

B. Optical Properties

Optical measurements were made to examine crystal composition and quality. First, the optical absorption was measured at room temperature across the bandgap (Fig. 2). The absorption edge was observed to be quite broad as would be expected at room temperature due to phonon-assisted processes. The absorption edge was in the vicinity of 3.35 eV, where the GaN bandgap has been previously reported. [30]

Laser photoluminescence measurements were made on one epitaxial sample (No. 9301), but very little luminescence was observed.[31] This result suggests that nonradiative transitions are being made through a high density of impurities or defects.

C. Electrical Measurements

Contact resistance between the GaIn metallization and the film generally improved by 1-2 orders of magnitude during heating to and annealing at 600°C for periods up to 15 min. in the probe station at 10^{-1} Pa. In the case of the higher-resistivity, undoped films, film resistance was dominant after the anneal, whereas in the case of the lower-resistivity, Be-doped films, contact resistance remained dominant. Both resistances increased rapidly with decreasing temperature, so that all measurements were made at 600°C except for No. 9301.

Table I shows 4-point resistivity measurements at 600°C for two undoped and three Be-doped films. The undoped films average just over two orders of magnitude higher in resistivity than the Be-doped films. The variation in resistivity with growth conditions within each of these two

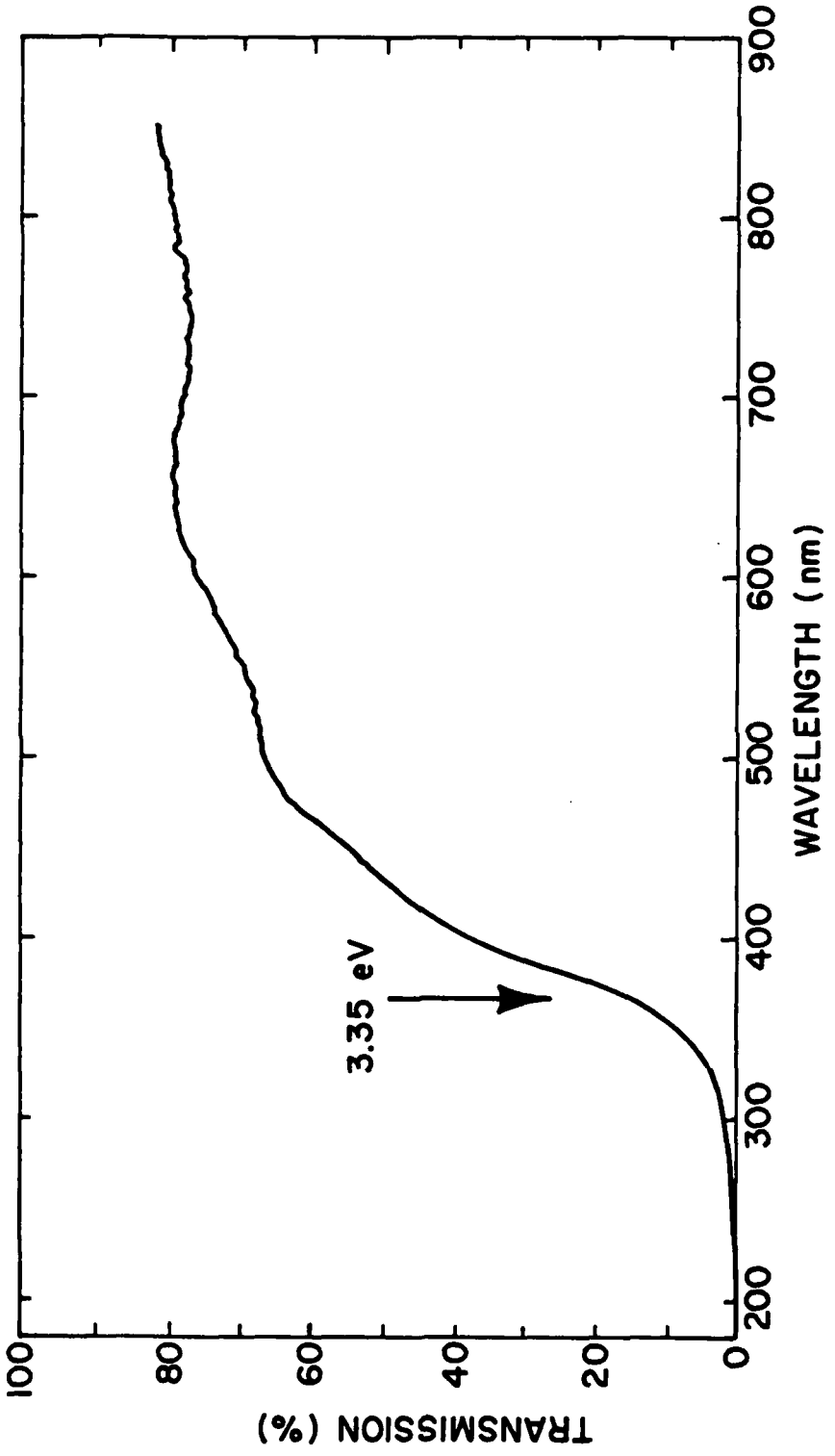

Figure 2. Fundamental Optical Absorption Edge of Sputter-Deposited GaN Film No. 7292.

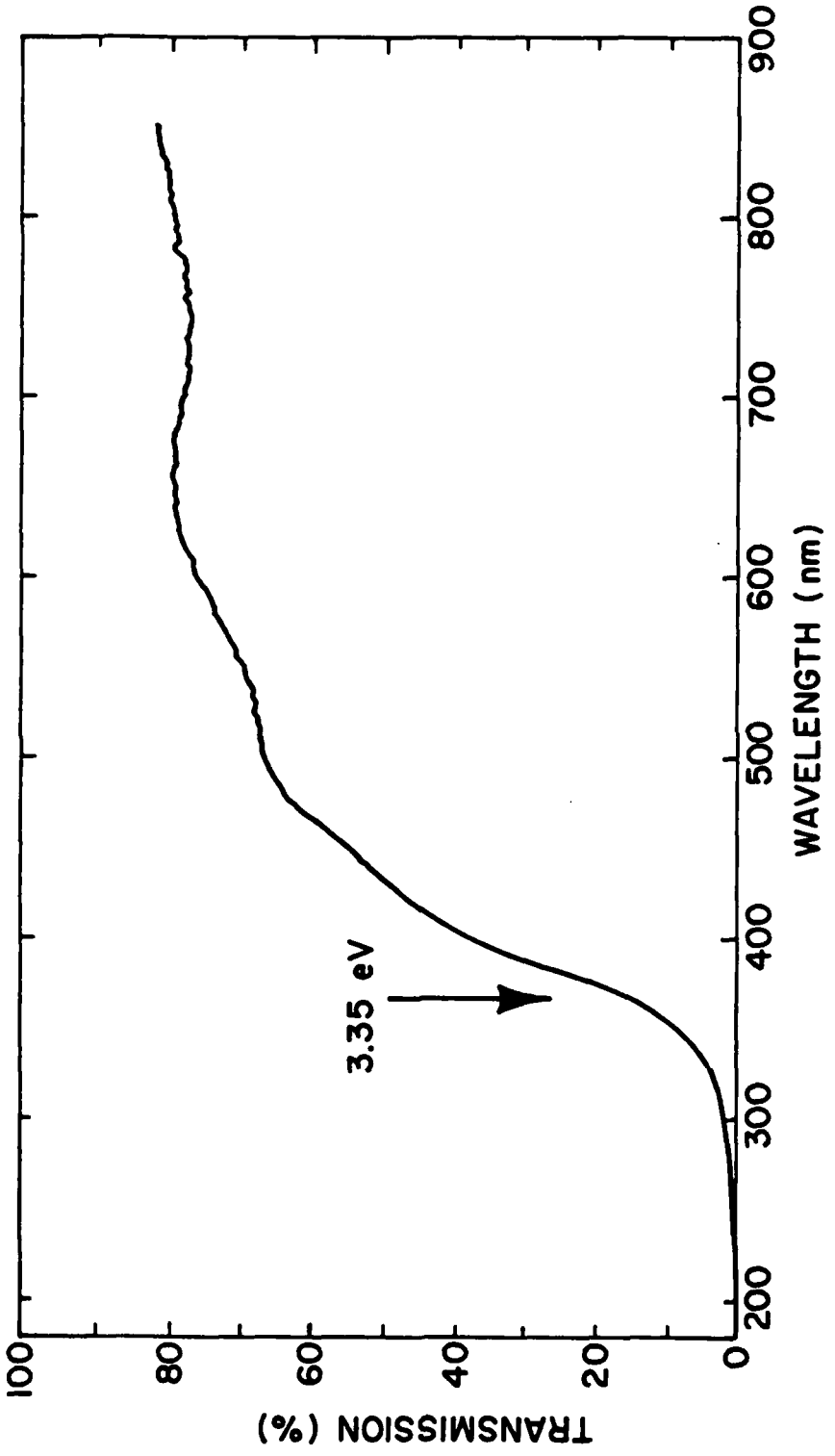

Figure 2. Fundamental Optical Absorption Edge of Sputter-Deposited GaN Film No. 7292.

groups would require more data to substantiate. Measurements on remaining films were invalidated by ground leakage interference. Attempts to measure the Hall voltage at 600°C of the Be-doped films and of No. 9301 did not result in signals that were above the noise level. For the Be-doped films, contact noise resulted in minimum detectable mobility of 60 cm^2/V-sec. No. 9301 yielded more stable signals and a detection limit of 5cm^2/V-sec. The resistivity of No. 9301 was also measured at lower temperatures, and Fig. 3 shows a plot of log(P) vs. 1/°K. Making the usual assumption of charge carriers which exhibit an activation energy for conduction, E_a, such that the fraction activated is proportional to $\exp(-E_a/kT)$, the slope in Fig. 3 decreases from that equivalent to E_a= 0.85 eV at 600°C to E_a= 0.2? eV at 300°C.

Carrier type was determined by thermoelectric probing when Hall voltage proved too low to determine type by that method. All four Be-doped films and the Sn-doped film gave a distinct negative current deflection at the cold probe (positive at the hot probe), indicating dominance of n-type conductivity.

groups would require more data to substantiate. Measurements on remaining films were invalidated by ground leakage interference. Attempts to measure the Hall voltage at 600°C of the Be-doped films and of No. 9301 did not result in signals that were above the noise level. For the Be-doped films, contact noise resulted in minimum detectable mobility of 60 cm^2/V-sec. No. 9301 yielded more stable signals and a detection limit of 5cm^2/V-sec. The resistivity of No. 9301 was also measured at lower temperatures, and Fig. 3 shows a plot of log(P) vs. 1/°K. Making the usual assumption of charge carriers which exhibit an activation energy for conduction, E_a, such that the fraction activated is proportional to $\exp(-E_a/kT)$, the slope in Fig. 3 decreases from that equivalent to E_a= 0.85 eV at 600°C to E_a= 0.2? eV at 300°C.

Carrier type was determined by thermoelectric probing when Hall voltage proved too low to determine type by that method. All four Be-doped films and the Sn-doped film gave a distinct negative current deflection at the cold probe (positive at the hot probe), indicating dominance of n-type conductivity.

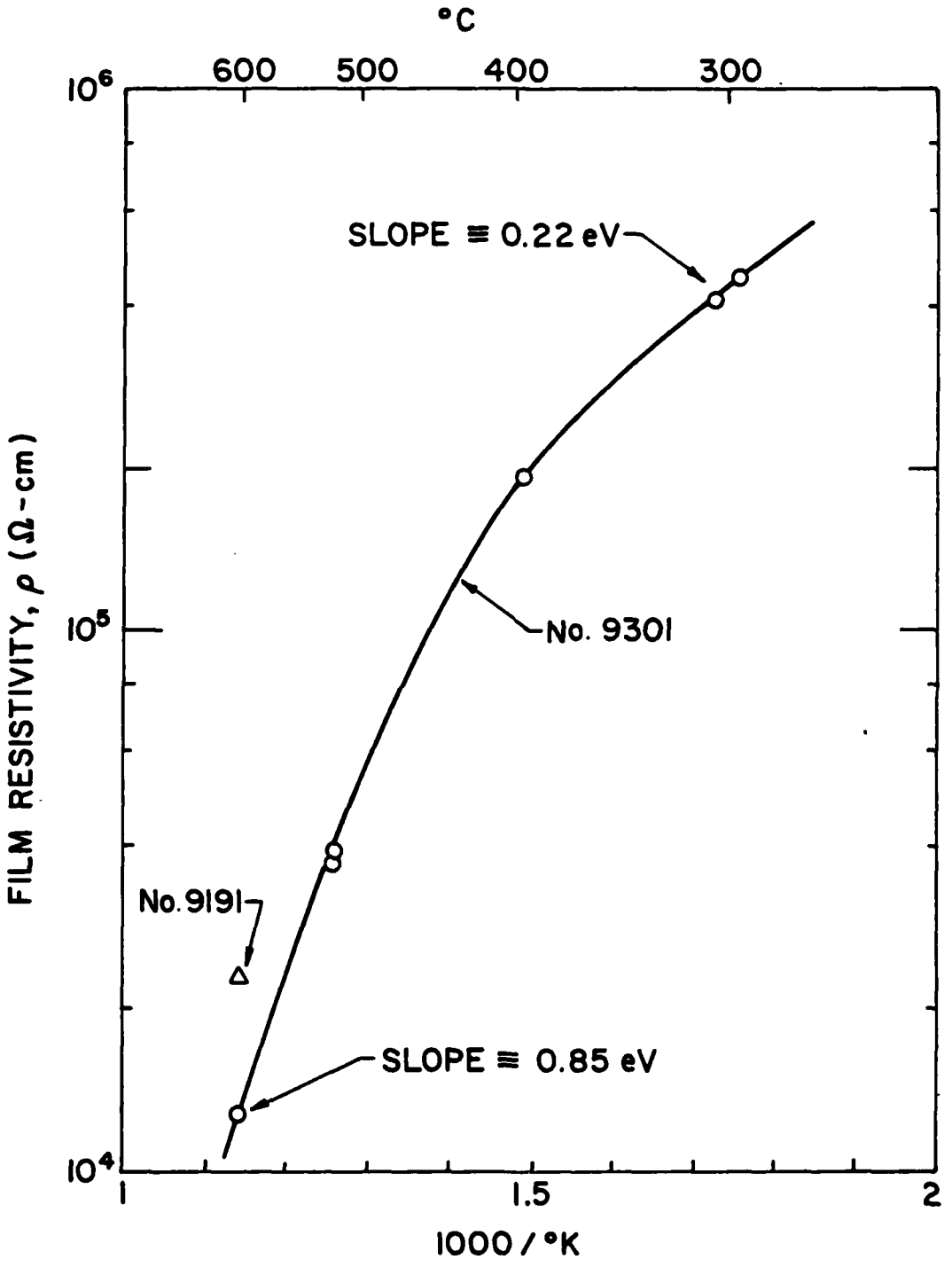

Figure 3. Dependence of GaN Film Resistivity on Temperature

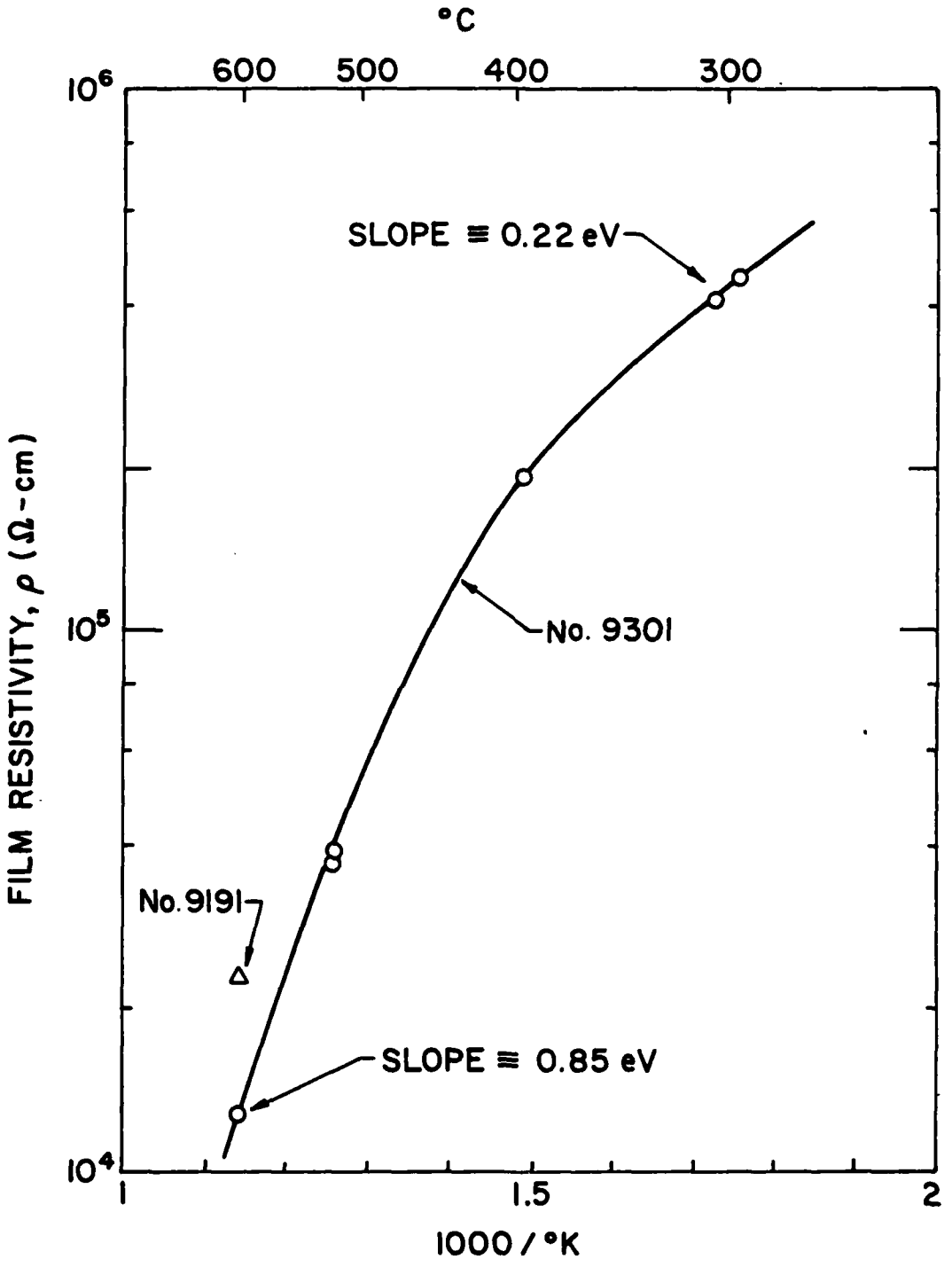

Figure 3. Dependence of GaN Film Resistivity on Temperature

IV. CONCLUSIONS

High-pressure (100 Pa) reactive sputtering of Ga in N_2 has been demonstrated as a viable technique for the deposition of GaN. Epitaxy on sapphire (0001) is obtained at 700°C but not at 500°C. This is similar to the result for deposition from Ga and active N_2 beams,[26] in which epitaxy was obtained at 600°C but not below 550°C. The major difference in the present work is that the active N_2 pressure at the growth surface is about 10^5 higher. Epitaxy is lost at 700°C by incorporation of high ($4\text{-}6\times10^{20}/cm^3$) Be doping (film no. #11181). GaN growth by evaporation of Ga into a N_2 plasma at similar pressures could not be controlled to give reproducible deposits.

While optical absorbtion (Fig. 2) shows that the sputtered GaN exhibits the proper bandgap, and Auger spectroscopy verifies Ga and N as the major constituents, other evidence suggests that the films contain substantial contamination or disorder. The mobility of <5 cm^2/V-sec. for film no. #9301 indicates extensive carrier scattering by such defects even though the film is epitaxial, and the weak photoluminescence observed for the same film suggests defects which are causing nonradiative recombination. The activation energy, E_a, of electrically active defects was calculated from the resistivity (ρ) data of Fig. 3 and was found to vary from 0.22 to 0.85 eV with increasing temperature, indicating at least two energy levels. Similarly large E_a and low mobility was found by Yaney,[27] (Table I) though E_a did not vary with measurement temperature and ρ was lower than ours, the latter probably due to the much lower overpressure of active N_2.

The x100 drop in ρ and n-type thermoelectric effect caused by Be doping means that Be is behaving predominantly as a donor. Since Be_{Ga} would be expected to be a shallow acceptor and Be_N a deep acceptor, the electrically active Be must reside here in an interstitial site where donor behavior would be expected, or in some sort of complex. Previous attempts to p-dope GaN have resulted in <u>increased</u> resistivity, presumably due to self-compensation. The present result suggests that Be is not acting as a self-compensated acceptor, but rather as a donor. Because of

IV. CONCLUSIONS

High-pressure (100 Pa) reactive sputtering of Ga in N_2 has been demonstrated as a viable technique for the deposition of GaN. Epitaxy on sapphire (0001) is obtained at 700°C but not at 500°C. This is similar to the result for deposition from Ga and active N_2 beams,[26] in which epitaxy was obtained at 600°C but not below 550°C. The major difference in the present work is that the active N_2 pressure at the growth surface is about 10^5 higher. Epitaxy is lost at 700°C by incorporation of high ($4\text{-}6\times10^{20}/cm^3$) Be doping (film no. #11181). GaN growth by evaporation of Ga into a N_2 plasma at similar pressures could not be controlled to give reproducible deposits.

While optical absorbtion (Fig. 2) shows that the sputtered GaN exhibits the proper bandgap, and Auger spectroscopy verifies Ga and N as the major constituents, other evidence suggests that the films contain substantial contamination or disorder. The mobility of <5 cm^2/V-sec. for film no. #9301 indicates extensive carrier scattering by such defects even though the film is epitaxial, and the weak photoluminescence observed for the same film suggests defects which are causing nonradiative recombination. The activation energy, E_a, of electrically active defects was calculated from the resistivity (ρ) data of Fig. 3 and was found to vary from 0.22 to 0.85 eV with increasing temperature, indicating at least two energy levels. Similarly large E_a and low mobility was found by Yaney,[27] (Table I) though E_a did not vary with measurement temperature and ρ was lower than ours, the latter probably due to the much lower overpressure of active N_2.

The x100 drop in ρ and n-type thermoelectric effect caused by Be doping means that Be is behaving predominantly as a donor. Since Be_{Ga} would be expected to be a shallow acceptor and Be_N a deep acceptor, the electrically active Be must reside here in an interstitial site where donor behavior would be expected, or in some sort of complex. Previous attempts to p-dope GaN have resulted in <u>increased</u> resistivity, presumably due to self-compensation. The present result suggests that Be is not acting as a self-compensated acceptor, but rather as a donor. Because of

this behavior, we cannot establish whether or not the self-compensation reaction has been frozen or reversed by the special growth conditions which we have established.

In order to improve chances of observing p-type behavior for Be in GaN, it would be advisable to take additional precautions to insure low unintentional impurity content in the deposit and to introduce Be over a range of lower concentrations. Both of these steps would reduce the possibility of complex formation, as well as improving crystal quality and electrical transport. SIMS analysis of impurity content and reaction chamber redesign to minimze sputtering of impurities are recommended. If n-type behavior is still seen, other potential p-dopants should be investigated.

Hope for overcoming the self-compensation problem is provided by the recent demonstration of this achievement in Zn_3P_2, where interstitial P acceptors appear to compensate impurity n-dopants. The use of Mg, diffused into interstitial donor sites at very low temperature (125°C) has resulted in n-type material.[32] It may nevertheless turn out that there exist no shallow acceptors for GaN or (AlGa)N. Photoluminescence studies of 35 elements ion-implanted into GaN and annealed in NH_3 at 1050°C showed deep levels for all, including all of the groups IIA and B elements.[33] Deep levels have also been found for Be[34,35] and for Zn and Cd[36] incorporated during CVD growth. Even if the self-compensation reaction can be brought under control, these high-bandgap III-V semiconductors may remain dominated by unavoidable deep traps.

this behavior, we cannot establish whether or not the self-compensation reaction has been frozen or reversed by the special growth conditions which we have established.

In order to improve chances of observing p-type behavior for Be in GaN, it would be advisable to take additional precautions to insure low unintentional impurity content in the deposit and to introduce Be over a range of lower concentrations. Both of these steps would reduce the possibility of complex formation, as well as improving crystal quality and electrical transport. SIMS analysis of impurity content and reaction chamber redesign to minimze sputtering of impurities are recommended. If n-type behavior is still seen, other potential p-dopants should be investigated.

Hope for overcoming the self-compensation problem is provided by the recent demonstration of this achievement in Zn_3P_2, where interstitial P acceptors appear to compensate impurity n-dopants. The use of Mg, diffused into interstitial donor sites at very low temperature (125°C) has resulted in n-type material.[32] It may nevertheless turn out that there exist no shallow acceptors for GaN or (AlGa)N. Photoluminescence studies of 35 elements ion-implanted into GaN and annealed in NH_3 at 1050°C showed deep levels for all, including all of the groups IIA and B elements.[33] Deep levels have also been found for Be[34,35] and for Zn and Cd[36] incorporated during CVD growth. Even if the self-compensation reaction can be brought under control, these high-bandgap III-V semiconductors may remain dominated by unavoidable deep traps.

REFERENCES

1. J.I. Pankove, H.P. Maruska, J.E. Berkeyheiser, Appl. Phys. Lett. 17, 197 (1970).

2. U. Martinelli and J.I. Pankove, Appl. Phys. Lett. 25, 549 (1974).

3. R.L. Bell and W.E. Spicer, Proc. IEEE 58, 1788 (1970).

4. A.I. Dirochka, M.N. Zargar'yants, A.A. Kiselev, and E.V. Sinitsyn, Sov. Phys. Semicond. 13, 113 (1979).

5. A.N. Pikhtin, E.B. Sokolov, A.V. Solomonov, and V.P. Chegnov, Sov. Phys. Semicond. 13, 1182 (1979).

6. J. Edward, K. Kawabe, G. Stevens, and R.H. Tredgold, Solid State Commun. 3, 99 (1965).

7. T.L. Chu, D.W. Ing, and A.J. Noreika, Solid State Electron, 10, 1023 (1967).

8. F.R. Brebrick in "Progress in Solid State Chemisty" 3, 213 (Pergamon, 1967).

9. J.A. Van Vechten, J. Electrochem. Soc. 122, 419 (1975); 122, 423 (1975).

10. C.D. Thurmond and R.A. Logan, J. Electrochem. Soc. 119, 622 (1972).

11. G. Mandel, F.F. Morehead, and P.R. Wagner, Phys. Rev. 136, A826 (1964).

12. G.F. Neumark, J. Appl. Phys. 51, 3383 (1980).

13. J.P. Maruska and J.J. Tietjen; Appl. Phys. Let. 15, 327 (1969).

14. R. Dingle, D.D. Sell, S.E. Stokowski, and M.Ilegems; Phys. Rev. B4 1211 (1971).

15. A.S. Barker and M.Ilegems; Phys. Rev. B7, 743 (1973).

16. T.L. Chu and K.Ito; J. Electrochem Soc. 121, 159 (1974).

17. R. Lappa, G. Glowacki, and S. Galkowski; Thin Solid Films 32, 73 (1976).

18. M. Gershnezon; "Evaluation of GaN for Active Microwave Devices", contract report no. #N00014-75-C-0295 (U. of S. Calif., 1975).

19. H.M. Manasevit, F.M. Erdmann and W.I. Simpson; J. Electrochem Soc. 118, 1864 (1971).

20. K.C. Wiemer; "Reactive Plasma Deposition of GaN epitaxial Layers", contract report no. #N00014-73-C-0054 (Texas Inst., Dallas, 1973).

REFERENCES

1. J.I. Pankove, H.P. Maruska, J.E. Berkeyheiser, Appl. Phys. Lett. 17, 197 (1970).

2. U. Martinelli and J.I. Pankove, Appl. Phys. Lett. 25, 549 (1974).

3. R.L. Bell and W.E. Spicer, Proc. IEEE 58, 1788 (1970).

4. A.I. Dirochka, M.N. Zargar'yants, A.A. Kiselev, and E.V. Sinitsyn, Sov. Phys. Semicond. 13, 113 (1979).

5. A.N. Pikhtin, E.B. Sokolov, A.V. Solomonov, and V.P. Chegnov, Sov. Phys. Semicond. 13, 1182 (1979).

6. J. Edward, K. Kawabe, G. Stevens, and R.H. Tredgold, Solid State Commun. 3, 99 (1965).

7. T.L. Chu, D.W. Ing, and A.J. Noreika, Solid State Electron, 10, 1023 (1967).

8. F.R. Brebrick in "Progress in Solid State Chemisty" 3, 213 (Pergamon, 1967).

9. J.A. Van Vechten, J. Electrochem. Soc. 122, 419 (1975); 122, 423 (1975).

10. C.D. Thurmond and R.A. Logan, J. Electrochem. Soc. 119, 622 (1972).

11. G. Mandel, F.F. Morehead, and P.R. Wagner, Phys. Rev. 136, A826 (1964).

12. G.F. Neumark, J. Appl. Phys. 51, 3383 (1980).

13. J.P. Maruska and J.J. Tietjen; Appl. Phys. Let. 15, 327 (1969).

14. R. Dingle, D.D. Sell, S.E. Stokowski, and M.Ilegems; Phys. Rev. B4 1211 (1971).

15. A.S. Barker and M.Ilegems; Phys. Rev. B7, 743 (1973).

16. T.L. Chu and K.Ito; J. Electrochem Soc. 121, 159 (1974).

17. R. Lappa, G. Glowacki, and S. Galkowski; Thin Solid Films 32, 73 (1976).

18. M. Gershnezon; "Evaluation of GaN for Active Microwave Devices", contract report no. #N00014-75-C-0295 (U. of S. Calif., 1975).

19. H.M. Manasevit, F.M. Erdmann and W.I. Simpson; J. Electrochem Soc. 118, 1864 (1971).

20. K.C. Wiemer; "Reactive Plasma Deposition of GaN epitaxial Layers", contract report no. #N00014-73-C-0054 (Texas Inst., Dallas, 1973).

21. K.K. Yee in "Proc. 5th Internat. Conf. on CVD" (Electrochem Soc., Princeton, NJ 1975); p. 283.

22. R. Madar, G. Jacob, J. Hallais, and R. Fruchart, J. Crystal Growth 31, 197 (1975).

23. G. Jacob, M. Boulou, M. Furtado, and D. Bois, J. Electronic Mater. 7, 499 (1978).

24. H.J. Hovel and J.J. Cuomo; Appl. Phys. Let. 20, 71 (1972).

25. T. Hariu, T. Usuba, H. Adachi, Y. Shibata; Appl. Phys. Lett 32, 252 (1978).

26. B.B. Kosicki and D. Kahng; J. Vac. Sci. & Tech. 6 593 (1969).

27. D.S. Yaney, Ph.D Thesis, Rensselaer Polytechnic Institute, Troy, N.Y. (Sept. 1977).

28. Private conversations with H.P. Broida, U. of California, Santa Barbara (1979).

29. J. Berkowitz, W.A. Chupka, and D.H. Kistiakowsky, J. Chem. Phys. 25, 457 (1956).

30. J.I. Pankove & S. Bloom, RCA Review 36, 163 (1975).

31. Measurements made by J.I. Pankove at RCA Laboratory. (1980).

32. A. Catalano and M. Bhushan; Appl. Phys. Lett. 37, 567 (1980).

33. J.I. Pankove and J.A. Hutchby; J. Appl. Phys. 47, 5387 (1976).

34. M. Ilegems and R. Dingle, Journal of Applied Physics, 44, 4234 (1973).

35. M. Ilegems, R. Dingle and R. Logan, Journal of Applied Physics, 43, 3797 (1972).

36. O. Lagerstadt and B. Monemar, Journal of Applied Physics, 45, 2266 (1974).

21. K.K. Yee in "Proc. 5th Internat. Conf. on CVD" (Electrochem Soc., Princeton, NJ 1975); p. 283.

22. R. Madar, G. Jacob, J. Hallais, and R. Fruchart, J. Crystal Growth 31, 197 (1975).

23. G. Jacob, M. Boulou, M. Furtado, and D. Bois, J. Electronic Mater. 7, 499 (1978).

24. H.J. Hovel and J.J. Cuomo; Appl. Phys. Let. 20, 71 (1972).

25. T. Hariu, T. Usuba, H. Adachi, Y. Shibata; Appl. Phys. Lett 32, 252 (1978).

26. B.B. Kosicki and D. Kahng; J. Vac. Sci. & Tech. 6 593 (1969).

27. D.S. Yaney, Ph.D Thesis, Rensselaer Polytechnic Institute, Troy, N.Y. (Sept. 1977).

28. Private conversations with H.P. Broida, U. of California, Santa Barbara (1979).

29. J. Berkowitz, W.A. Chupka, and D.H. Kistiakowsky, J. Chem. Phys. 25, 457 (1956).

30. J.I. Pankove & S. Bloom, RCA Review 36, 163 (1975).

31. Measurements made by J.I. Pankove at RCA Laboratory. (1980).

32. A. Catalano and M. Bhushan; Appl. Phys. Lett. 37, 567 (1980).

33. J.I. Pankove and J.A. Hutchby; J. Appl. Phys. 47, 5387 (1976).

34. M. Ilegems and R. Dingle, Journal of Applied Physics, 44, 4234 (1973).

35. M. Ilegems, R. Dingle and R. Logan, Journal of Applied Physics, 43, 3797 (1972).

36. O. Lagerstadt and B. Monemar, Journal of Applied Physics, 45, 2266 (1974).

APPENDIX A

Negative Electron Affinity Photoemission

In semiconductors designed for photoemission, incoming photons are absorbed primarily by transferring their energy to valence-band electrons, which are thereby excited into the conduction band. These hot electrons lose energy rapidly by scattering processes until they arrive at the bottom of the conduction band, at which time they are said to be thermalized. In a conventional photoemitter,[A1] thermalized electrons cannot escape into the vacuum because of the energy barrier imposed by the electron affinity, E_a, of the semiconductor, as seen in Fig. Ala. Only photogenerated electrons having energy $h\nu > E_g + E_a$ when they reach the surface will be able to escape, where E_a is the band-gap energy. Electrons generated by photons having energies only slightly above the threshold ($E_g + E_a$) can therefore escape only if they are generated very close to the surface, on the order of tens of angstroms. Since most photons penetrate more deeply than this before being absorbed, quantum efficiency is low near threshold and rises slowly as photon energy increases, resulting in a broad cut-off characteristic. The cut-off is further broadened by variations in E_a over the photoemissive surface. The E_a of a semiconductor is influenced by the structure and chemistry at the surface just as is the work function of a metal.

NEA photoemitters, on the other hand, consist of a p-doped semiconductor covered with a few monolayers of a low-work-function coating such as Cs_2O. The Cs_2O contributes electrons to the semiconductor substrate, causing the bands to bend down near the surface as shown in Figure Alb. (The NEA photoemission process has been extensively analyzed in the literature[A2,A3]). If E_g is large enough, the vacuum level can actually be below the bottom of the conduction band, so that even completely thermalized electrons can escape into the vacuum. The results is high quantum efficiency near threshold. Moreover, threshold is now equal to E_g, a fixed property of the bulk material, and is not affected by fluctuations in E_a over the surface as long as E_a remains negative. The result is a very sharp cut-off comparable in shape to

APPENDIX A

Negative Electron Affinity Photoemission

In semiconductors designed for photoemission, incoming photons are absorbed primarily by transferring their energy to valence-band electrons, which are thereby excited into the conduction band. These hot electrons lose energy rapidly by scattering processes until they arrive at the bottom of the conduction band, at which time they are said to be thermalized. In a conventional photoemitter,[A1] thermalized electrons cannot escape into the vacuum because of the energy barrier imposed by the electron affinity, E_a, of the semiconductor, as seen in Fig. Ala. Only photogenerated electrons having energy $h\nu > E_g + E_a$ when they reach the surface will be able to escape, where E_a is the band-gap energy. Electrons generated by photons having energies only slightly above the threshold ($E_g + E_a$) can therefore escape only if they are generated very close to the surface, on the order of tens of angstroms. Since most photons penetrate more deeply than this before being absorbed, quantum efficiency is low near threshold and rises slowly as photon energy increases, resulting in a broad cut-off characteristic. The cut-off is further broadened by variations in E_a over the photoemissive surface. The E_a of a semiconductor is influenced by the structure and chemistry at the surface just as is the work function of a metal.

NEA photoemitters, on the other hand, consist of a p-doped semiconductor covered with a few monolayers of a low-work-function coating such as Cs_2O. The Cs_2O contributes electrons to the semiconductor substrate, causing the bands to bend down near the surface as shown in Figure Alb. (The NEA photoemission process has been extensively analyzed in the literature[A2,A3]). If E_g is large enough, the vacuum level can actually be below the bottom of the conduction band, so that even completely thermalized electrons can escape into the vacuum. The results is high quantum efficiency near threshold. Moreover, threshold is now equal to E_g, a fixed property of the bulk material, and is not affected by fluctuations in E_a over the surface as long as E_a remains negative. The result is a very sharp cut-off comparable in shape to

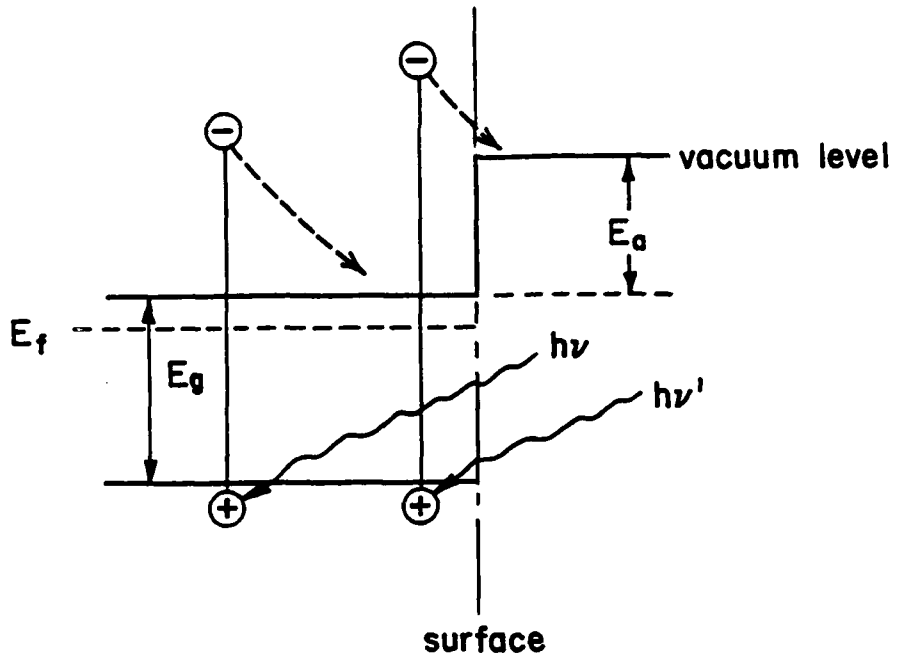

a. Conventional Photoemitter

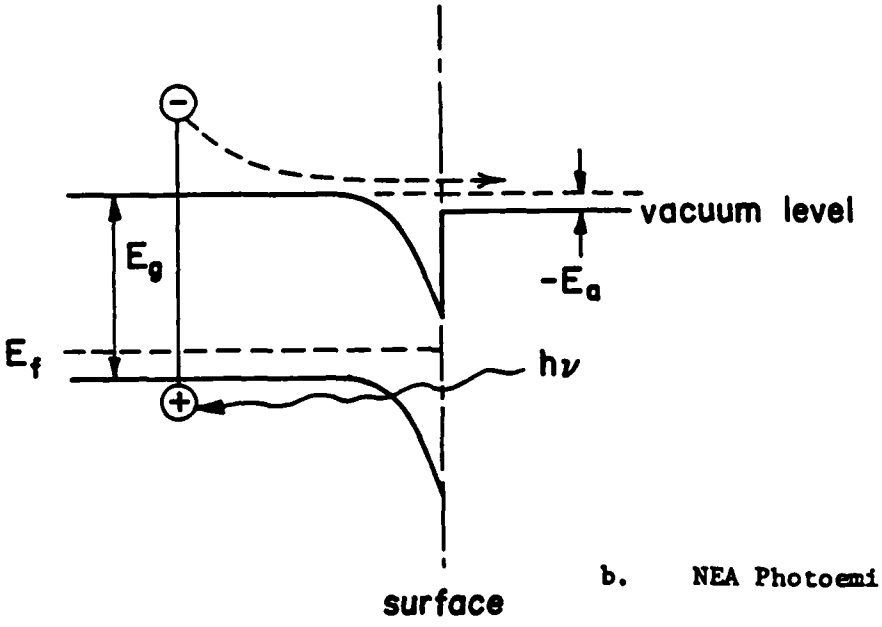

b. NEA Photoemitter

Figure A1 - Schematic Representations of Photoemission Processes
$h\nu$ = energy of near-threshold incident photon,
$h\nu'$ = energy of shorter-wavelength incident photon
E_F = Fermi level, E_g = bandgap, E_a = electron affinity

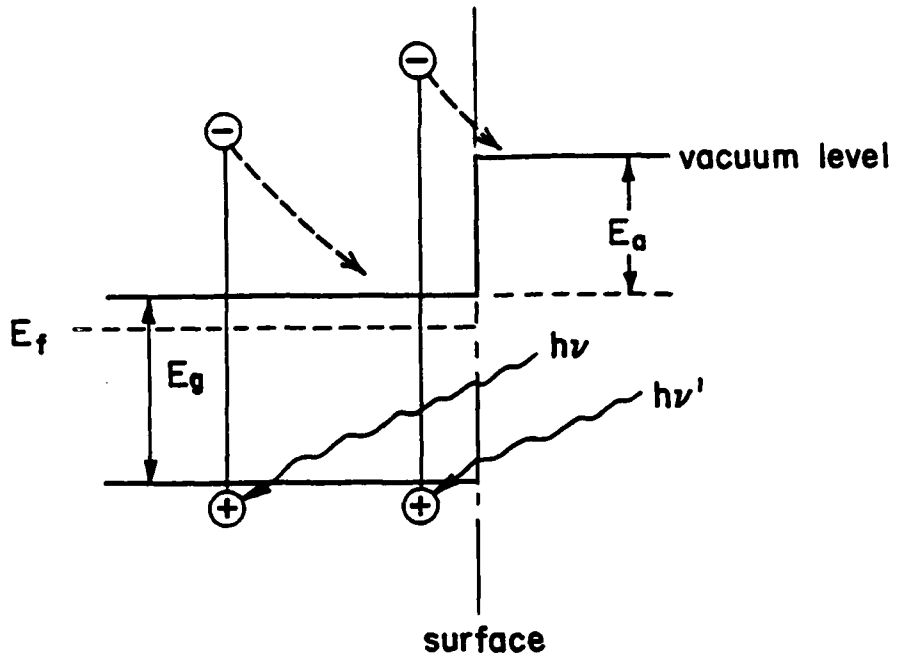

a. Conventional Photoemitter

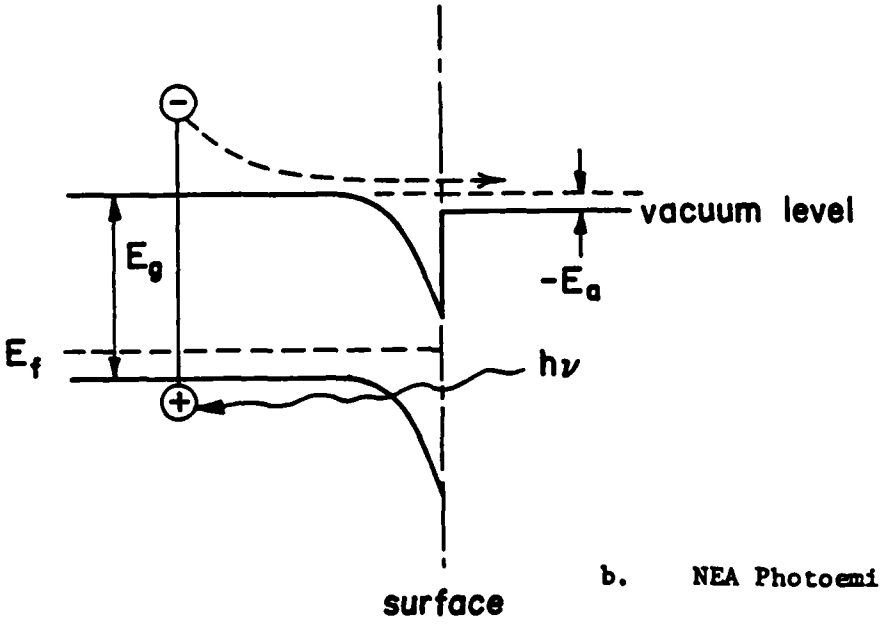

b. NEA Photoemitter

Figure A1 - Schematic Representations of Photoemission Processes
$h\nu$ = energy of near-threshold incident photon,
$h\nu'$ = energy of shorter-wavelength incident photon
E_F = Fermi level, E_g = bandgap, E_a = electron affinity

that of the fundamental optical absorption edge of the semiconductor material.

An appropriate semiconductor for NEA photoemission is one which can be p-doped to the 10^{18} cm^{-3} range and which preferably also has a direct bandgap. In indirect-bangap semiconductors, excitation of electrons across the bandgap by photon absorption can only take place when accompanied by a certain amount of momentum transfer (usually with a phonon). Since the probability of these two collisions happening simultaneously is much less than that of a direct transition in which momentum exchange is not involved, the absorption edge is much more broad and the photoemissive quantum efficiency much lower in indirect-gap than in direct-gap semiconductors. The III-V compund semiconductors have been by far the most widely exploited group of materials for NEA photoemission because many of them have direct bandgaps and because continuous band-gap tuneability is available by employing solid solutions such as $Ga_xIn_{1-x}As$.

A likely candidate for the near-UV regime is the III-V solution $Al_xGa_{1-x}N$. The bandgaps for GaN and AlN are 3.6 eV[A4] and 6.2 eV[A5], respectively, and they are both direct. Solution composition adjustment could thus provide photoemitter cutoffs from 0.20 to 0.34 micrometers. Approximate compositions for intermediate cutoff wavelengths can be calculated by assuming that the bandgap varies linearly with composition. For example, the composition of a photoemitter designed for solar-blind operation and having a cutoff of 0.29 micrometers would be $Al_{0.24}Ga_{0.76}N$.

GaN has in fact been activated to the NEA condition with Cs-O, and both secondary elecron emission[A6] and photoemission[A7] have been observed. The spectral response of this experimental photoemitter is plotted in Figure A2. Although cutoff is sharp, quantum efficiency near threshold is low. This is because the material used was not p-type, but rather "semi-insulating" material produced by compensating out a large concentration of n-type carriers with Zn dopant. Without high p-doping, the band-bending region near the photoemitter surface is much wider than shown in Figure Alb, causing re-acceleration to a "hot" state of thermalized photoexcited electrons at a depth large enough so that most of

that of the fundamental optical absorption edge of the semiconductor material.

An appropriate semiconductor for NEA photoemission is one which can be p-doped to the 10^{18} cm^{-3} range and which preferably also has a direct bandgap. In indirect-bangap semiconductors, excitation of electrons across the bandgap by photon absorption can only take place when accompanied by a certain amount of momentum transfer (usually with a phonon). Since the probability of these two collisions happening simultaneously is much less than that of a direct transition in which momentum exchange is not involved, the absorption edge is much more broad and the photoemissive quantum efficiency much lower in indirect-gap than in direct-gap semiconductors. The III-V compund semiconductors have been by far the most widely exploited group of materials for NEA photoemission because many of them have direct bandgaps and because continuous band-gap tuneability is available by employing solid solutions such as $Ga_xIn_{1-x}As$.

A likely candidate for the near-UV regime is the III-V solution $Al_xGa_{1-x}N$. The bandgaps for GaN and AlN are 3.6 eV[A4] and 6.2 eV[A5], respectively, and they are both direct. Solution composition adjustment could thus provide photoemitter cutoffs from 0.20 to 0.34 micrometers. Approximate compositions for intermediate cutoff wavelengths can be calculated by assuming that the bandgap varies linearly with composition. For example, the composition of a photoemitter designed for solar-blind operation and having a cutoff of 0.29 micrometers would be $Al_{0.24}Ga_{0.76}N$.

GaN has in fact been activated to the NEA condition with Cs-O, and both secondary elecron emission[A6] and photoemission[A7] have been observed. The spectral response of this experimental photoemitter is plotted in Figure A2. Although cutoff is sharp, quantum efficiency near threshold is low. This is because the material used was not p-type, but rather "semi-insulating" material produced by compensating out a large concentration of n-type carriers with Zn dopant. Without high p-doping, the band-bending region near the photoemitter surface is much wider than shown in Figure Alb, causing re-acceleration to a "hot" state of thermalized photoexcited electrons at a depth large enough so that most of

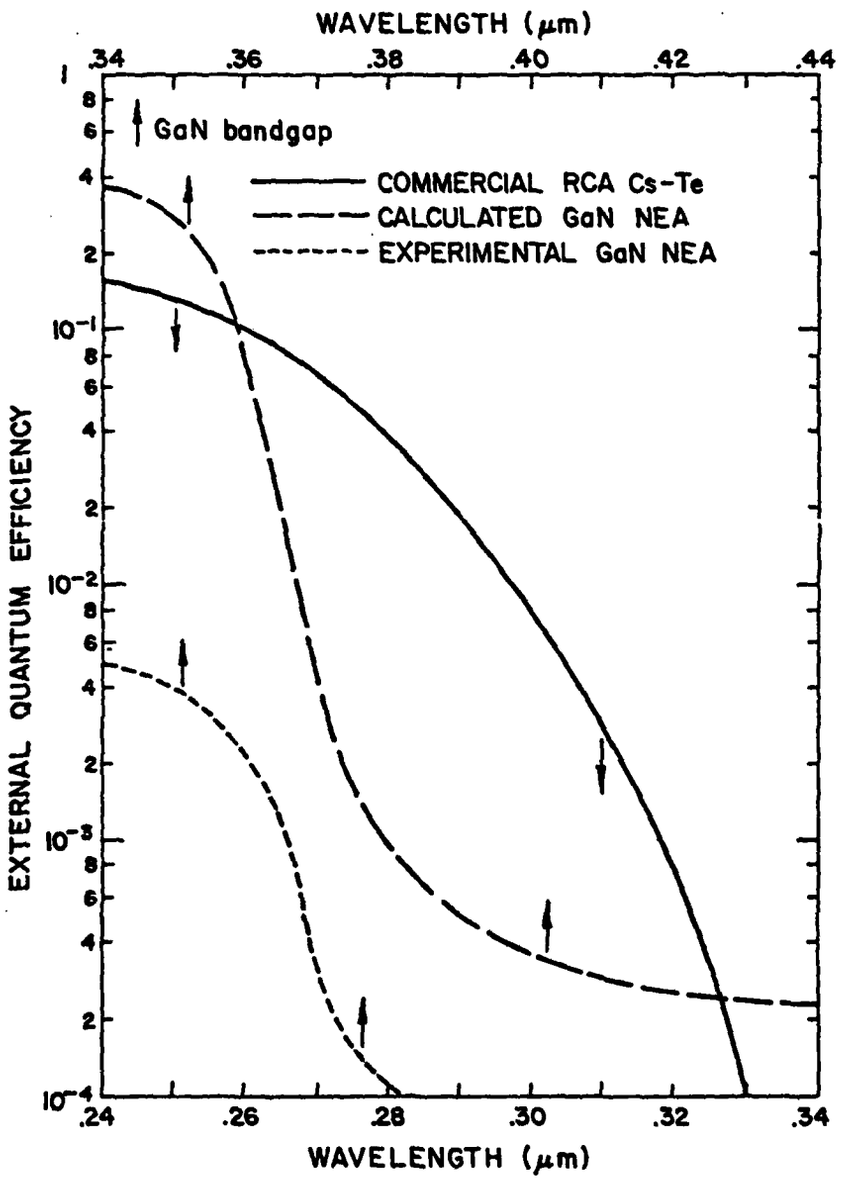

Figure A2. Spectral Response of Various UV Photoemitters

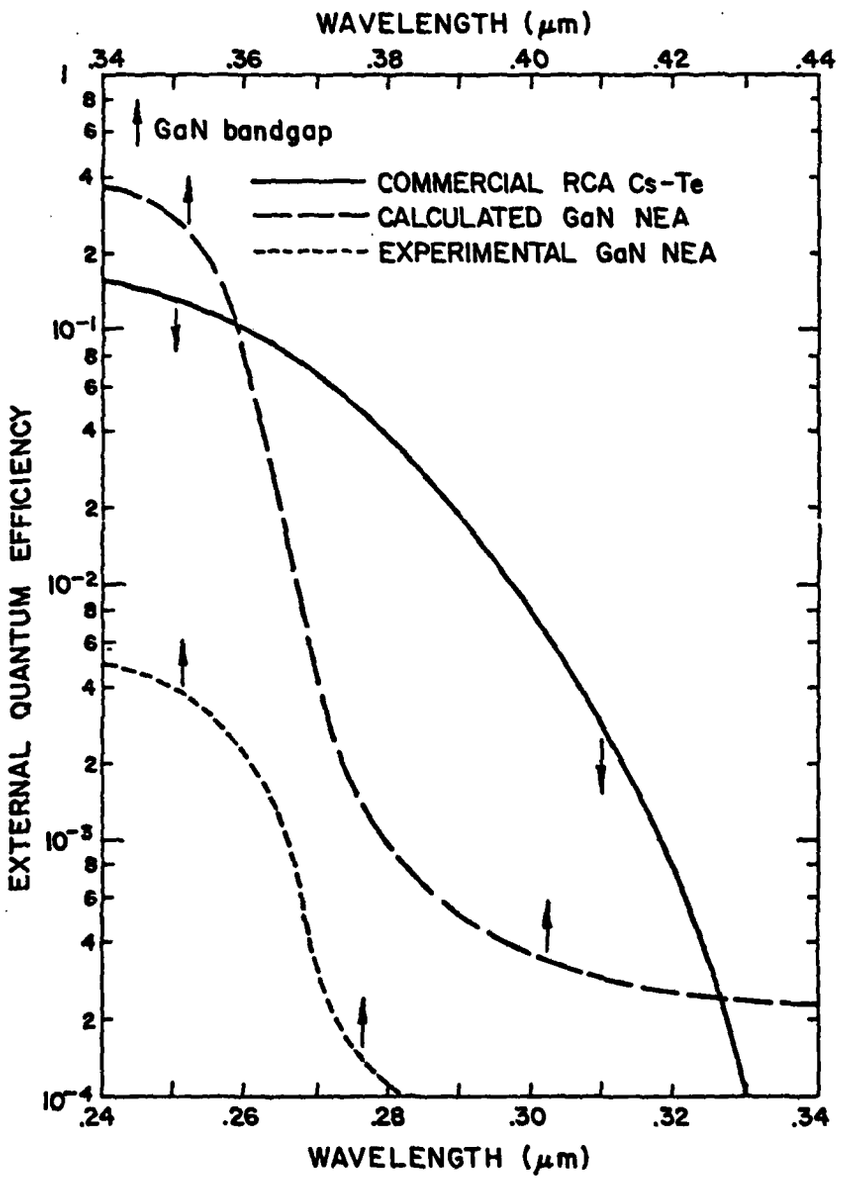

Figure A2. Spectral Response of Various UV Photoemitters

them suffer collisional losses before reaching the surface. The spectral response of a true NEA GaN photoemitter can be calculated from[A8]

$$QE = \int_0^\infty (1-R)\alpha\exp(-\alpha x - x/L)dx = (1-R)\alpha L/(\alpha L+1),$$

where Q= quantum efficiency, R= reflectivity (=0.19 for GaN[A12]), α= optical absorbtion coefficient[A9], x= depth from surface, and L= minority carrier diffusion length. Here L is taken as 100 angstroms, which is conservatively low compared to one estimate of 300-800 angstroms which has been made for this material.[A6] The αx and x/L exponential terms arise from the optical absorption and diffusion to the surface, respectively. Enhanced collection due to fields in the depletion region has been neglected, since this region is very narrow for high doping. The results of this calculation are plotted on Figure A2, along with the spectral response of the Cs-Te photoemitter (wavelength scale shifted) for comparison. The improvements in near-threshold quantum efficiency and especially in cutoff slope which can potentially made by using an NEA solar-blind photocathode are considerable. Whether or not there exists a semiconductor of appropriate direct bandgap which can be doped to 10^{18} P/cm^3 while retaining satisfactory transport properties remains to be seen.

them suffer collisional losses before reaching the surface. The spectral response of a true NEA GaN photoemitter can be calculated from[A8]

$$QE = \int_0^\infty (1-R)\alpha\exp(-\alpha x - x/L)dx = (1-R)\alpha L/(\alpha L+1),$$

where Q= quantum efficiency, R= reflectivity (=0.19 for GaN[A12]), α= optical absorbtion coefficient[A9], x= depth from surface, and L= minority carrier diffusion length. Here L is taken as 100 angstroms, which is conservatively low compared to one estimate of 300-800 angstroms which has been made for this material.[A6] The αx and x/L exponential terms arise from the optical absorption and diffusion to the surface, respectively. Enhanced collection due to fields in the depletion region has been neglected, since this region is very narrow for high doping. The results of this calculation are plotted on Figure A2, along with the spectral response of the Cs-Te photoemitter (wavelength scale shifted) for comparison. The improvements in near-threshold quantum efficiency and especially in cutoff slope which can potentially made by using an NEA solar-blind photocathode are considerable. Whether or not there exists a semiconductor of appropriate direct bandgap which can be doped to 10^{18} P/cm^3 while retaining satisfactory transport properties remains to be seen.

REFERENCES (Appendix A)

A1 A.H. Sommer; "Photoemissive Materials" (Wiley, NY, 1968); pg.9.

A2 J.J. Scheer and J. Van Laar; Solid State Commun. 3, 189 (1965).

A3 R.L. Bell and W.E. Spicer; Proc. IEEE 58, 1788 (1970).

A4 J.I. Pankove, S. Bloom, and G. Harbeke; RCA Rev. 36, 162 (1975).

A5 W.M. Kim, E.J. Stofko, P.J. Zanzucci, J.I. Pankove, M. Ettenberg, and S.L. Gilbert; J. Appl. Phys. 44, 292 (1973).

A6 R.U. Martinelli and J.I. Pankove; Appl. Phys. Let. 25, 549 (1974).

A7 J.I. Pankove and H. Schade; Appl. Phys. Let. 25, 53 (1974).

A8 H.J. Hovel, Semiconductors and Semimetals, V.11, p.115 (Academic, N.Y., 1975).

A9 J.I. Pankove, H.P. Maruska, and J.E. Berkeyheiser; Appl. Phys. Let. 17, 197 (1970).

REFERENCES (Appendix A)

A1 A.H. Sommer; "Photoemissive Materials" (Wiley, NY, 1968); pg.9.

A2 J.J. Scheer and J. Van Laar; Solid State Commun. 3, 189 (1965).

A3 R.L. Bell and W.E. Spicer; Proc. IEEE 58, 1788 (1970).

A4 J.I. Pankove, S. Bloom, and G. Harbeke; RCA Rev. 36, 162 (1975).

A5 W.M. Kim, E.J. Stofko, P.J. Zanzucci, J.I. Pankove, M. Ettenberg, and S.L. Gilbert; J. Appl. Phys. 44, 292 (1973).

A6 R.U. Martinelli and J.I. Pankove; Appl. Phys. Let. 25, 549 (1974).

A7 J.I. Pankove and H. Schade; Appl. Phys. Let. 25, 53 (1974).

A8 H.J. Hovel, Semiconductors and Semimetals, V.11, p.115 (Academic, N.Y., 1975).

A9 J.I. Pankove, H.P. Maruska, and J.E. Berkeyheiser; Appl. Phys. Let. 17, 197 (1970).

APPENDIX B

Reactive Evaporator Design

The maintenance of a stable, confined plasma in the 100 Pa range is much more difficult than at lower pressures where spurious plasmas are easily quenched by the use of insulation or ground shielding spaced closer than an electron mean free path to the electrodes. We first attempted to apply such techniques in the present work, being particularly careful about shielding tolerances in consideration of the much shorter mean free path at the higher pressure. Figures B1a and B1b show the two attempts which we made at such a design, using an inductively-coupled and a capacitively-coupled RF plasma respectively. In both cases, the electrodes were immersed in a vacuum chamber containing 100 Pa of N_2, which flowed up through the plasma between the electrodes after entraining the evaporated metal and then passed over the heated substrate. Great difficulty was encountered in preventing power from being coupled into plasmas elsewhere in the system than within the coil or between the electrodes, despite elaborate shielding consisting of ceramic wool, mica, and quartz.

Consequently, both approaches were finally abandoned in favor of the configuration shown in Figure B1c, in which the RF coil is external to the vacuum chamber. This configuration is more difficult to construct, because the region of the vacuum system between the evaporation source assembly and the substrate/exhaust chamber must be necked down to accommodate a close-fitting RF coil and must be fabricated from glass to pass the RF power. The constricted size also precluded the incorporation of auxiliary analytical facilities such as a quartz crystal deposition rate monitor. On the other hand, excellent plasma confinement in the reaction tube is achieved because the entire RF circuit operates at atmospheric pressure, where plasma generation is prevented by mean free paths so short that electrons cannot accelerate to energies sufficient to cause ionization.

APPENDIX B

Reactive Evaporator Design

The maintenance of a stable, confined plasma in the 100 Pa range is much more difficult than at lower pressures where spurious plasmas are easily quenched by the use of insulation or ground shielding spaced closer than an electron mean free path to the electrodes. We first attempted to apply such techniques in the present work, being particularly careful about shielding tolerances in consideration of the much shorter mean free path at the higher pressure. Figures B1a and B1b show the two attempts which we made at such a design, using an inductively-coupled and a capacitively-coupled RF plasma respectively. In both cases, the electrodes were immersed in a vacuum chamber containing 100 Pa of N_2, which flowed up through the plasma between the electrodes after entraining the evaporated metal and then passed over the heated substrate. Great difficulty was encountered in preventing power from being coupled into plasmas elsewhere in the system than within the coil or between the electrodes, despite elaborate shielding consisting of ceramic wool, mica, and quartz.

Consequently, both approaches were finally abandoned in favor of the configuration shown in Figure B1c, in which the RF coil is external to the vacuum chamber. This configuration is more difficult to construct, because the region of the vacuum system between the evaporation source assembly and the substrate/exhaust chamber must be necked down to accommodate a close-fitting RF coil and must be fabricated from glass to pass the RF power. The constricted size also precluded the incorporation of auxiliary analytical facilities such as a quartz crystal deposition rate monitor. On the other hand, excellent plasma confinement in the reaction tube is achieved because the entire RF circuit operates at atmospheric pressure, where plasma generation is prevented by mean free paths so short that electrons cannot accelerate to energies sufficient to cause ionization.

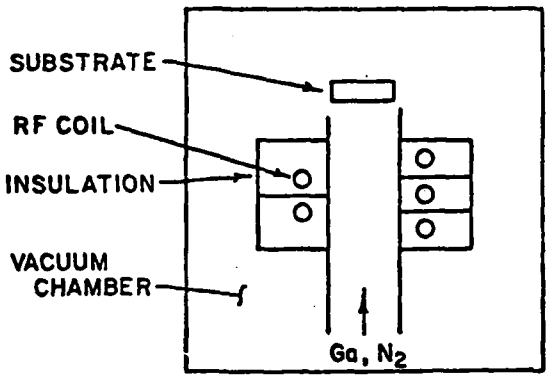

a. INDUCTIVE COUPLING WITH COIL IN 1 TORR N_2

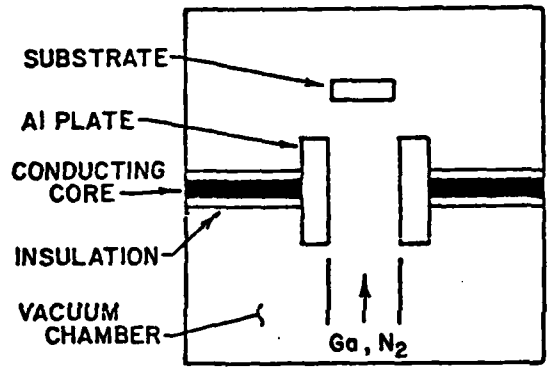

b. CAPACITIVE COUPLING WITH CAPACITOR IN 1 TORR N_2

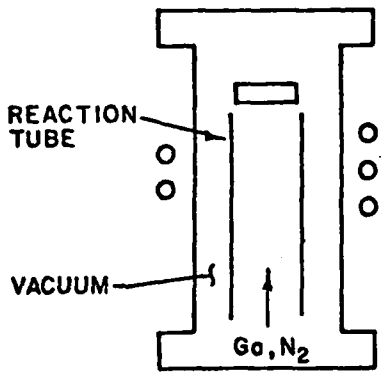

c. INDUCTIVE COUPLING WITH COIL OUT OF VACUUM

Figure B1. Approaches to Creating the Necessary Plasma Discharge Conditions for Reactive Evaporation of GaN

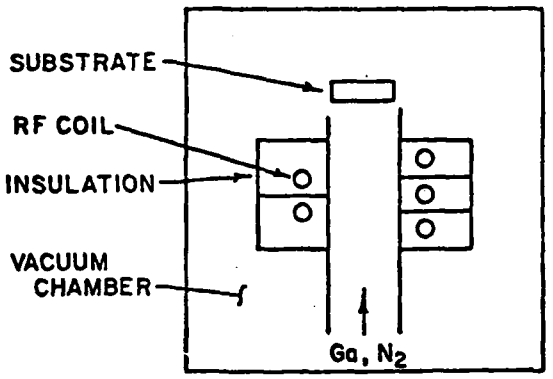

a. INDUCTIVE COUPLING WITH COIL IN 1 TORR N_2

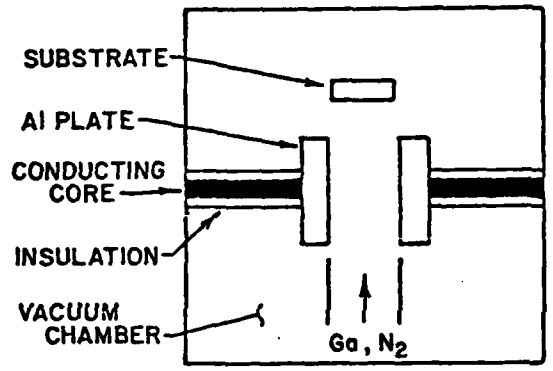

b. CAPACITIVE COUPLING WITH CAPACITOR IN 1 TORR N_2

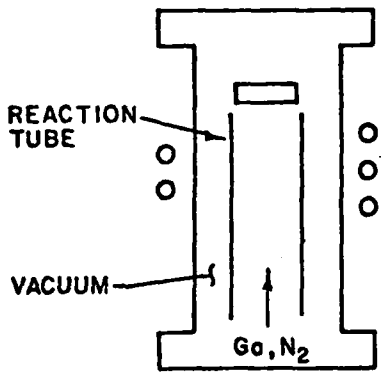

c. INDUCTIVE COUPLING WITH COIL OUT OF VACUUM

Figure B1. Approaches to Creating the Necessary Plasma Discharge Conditions for Reactive Evaporation of GaN

A more detailed schematic of the final reactor is shown in Figure B2. The discharge is confined by a pyrolytic BN tube so that the only contaminant which can be RF sputtered onto the film is B. In small amounts, B should not detrimentally affect the GaN, because it is expected to not be electrically active in GaN but to merely shift the bandgap slightly in substituting for Ga. Ultra-high vacuum (UHV) seals could not be made to the BN tube, so it was placed inside a glass tube as shown. The glass tube is sealed to a Kovar tube which is welded to a stainless steel UHV flange at each end to mate with the remainder of the stainless steel vacuum system. The annular region between the BN reaction tube and the glass vacuum jacket is packed with glass rods to prevent spurious discharges from occurring in that region. A water jacket surrounds the glass tube vacuum wall to prevent overheating by the RF discharge.

The N_2 is introduced at the bottom of the reactor and flows through the tube at a velocity of abouth 10m/sec. The Ga metal evaporant is introduced into the N_2 flow from a Knudsen cell evaporation source. This cell is made from a pyrolytic BN crucible, around which are wound coils of W wire. A Ta heat and RF shield is wrapped around the cell to reduce radiation loss and to provide RF shielding to a thermocouple which connects to the base of the crucible. The thermocouple allows control of the evaporant source to ±4°C at the 1100°C evaporating temperature, despite the intense RF discharge nearby, because of careful shielding and routing of the thermocouple wires. The mixture of N_2 and Ga flows through the RF discharge region where the reaction to GaN takes place.

At the downstream end of the BN tube, the substrate is sandwiched between a BN disk and a Mo-tipped Cu rod. Liquid Ga is used to insure good thermal contact between the substrate and the Mo tip. A heater and shielded thermocouple are attached to the Cu rod near the substrate, while the opposite end is temperature-sunk to the room. This arrangement allows close temperature control of the substrate during growth in the presence of the RF discharge. The Cu rod heat sink prevents substrate overheating by the discharge, and the heater and thermocouple are used in a feedback loop for temperature control.

A more detailed schematic of the final reactor is shown in Figure B2. The discharge is confined by a pyrolytic BN tube so that the only contaminant which can be RF sputtered onto the film is B. In small amounts, B should not detrimentally affect the GaN, because it is expected to not be electrically active in GaN but to merely shift the bandgap slightly in substituting for Ga. Ultra-high vacuum (UHV) seals could not be made to the BN tube, so it was placed inside a glass tube as shown. The glass tube is sealed to a Kovar tube which is welded to a stainless steel UHV flange at each end to mate with the remainder of the stainless steel vacuum system. The annular region between the BN reaction tube and the glass vacuum jacket is packed with glass rods to prevent spurious discharges from occurring in that region. A water jacket surrounds the glass tube vacuum wall to prevent overheating by the RF discharge.

The N_2 is introduced at the bottom of the reactor and flows through the tube at a velocity of abouth 10m/sec. The Ga metal evaporant is introduced into the N_2 flow from a Knudsen cell evaporation source. This cell is made from a pyrolytic BN crucible, around which are wound coils of W wire. A Ta heat and RF shield is wrapped around the cell to reduce radiation loss and to provide RF shielding to a thermocouple which connects to the base of the crucible. The thermocouple allows control of the evaporant source to ±4°C at the 1100°C evaporating temperature, despite the intense RF discharge nearby, because of careful shielding and routing of the thermocouple wires. The mixture of N_2 and Ga flows through the RF discharge region where the reaction to GaN takes place.

At the downstream end of the BN tube, the substrate is sandwiched between a BN disk and a Mo-tipped Cu rod. Liquid Ga is used to insure good thermal contact between the substrate and the Mo tip. A heater and shielded thermocouple are attached to the Cu rod near the substrate, while the opposite end is temperature-sunk to the room. This arrangement allows close temperature control of the substrate during growth in the presence of the RF discharge. The Cu rod heat sink prevents substrate overheating by the discharge, and the heater and thermocouple are used in a feedback loop for temperature control.

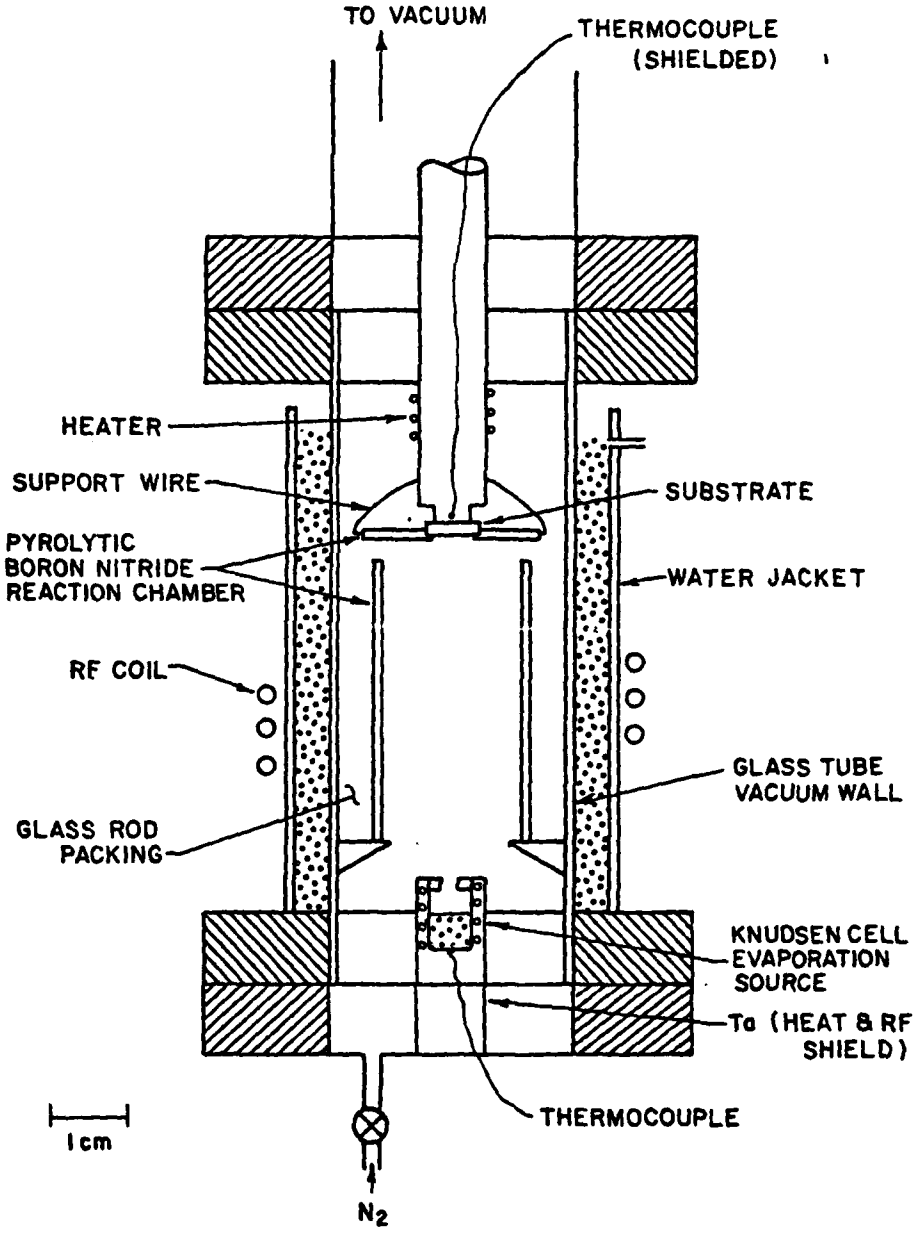

Figure B2. GaN Reactive Evaporator

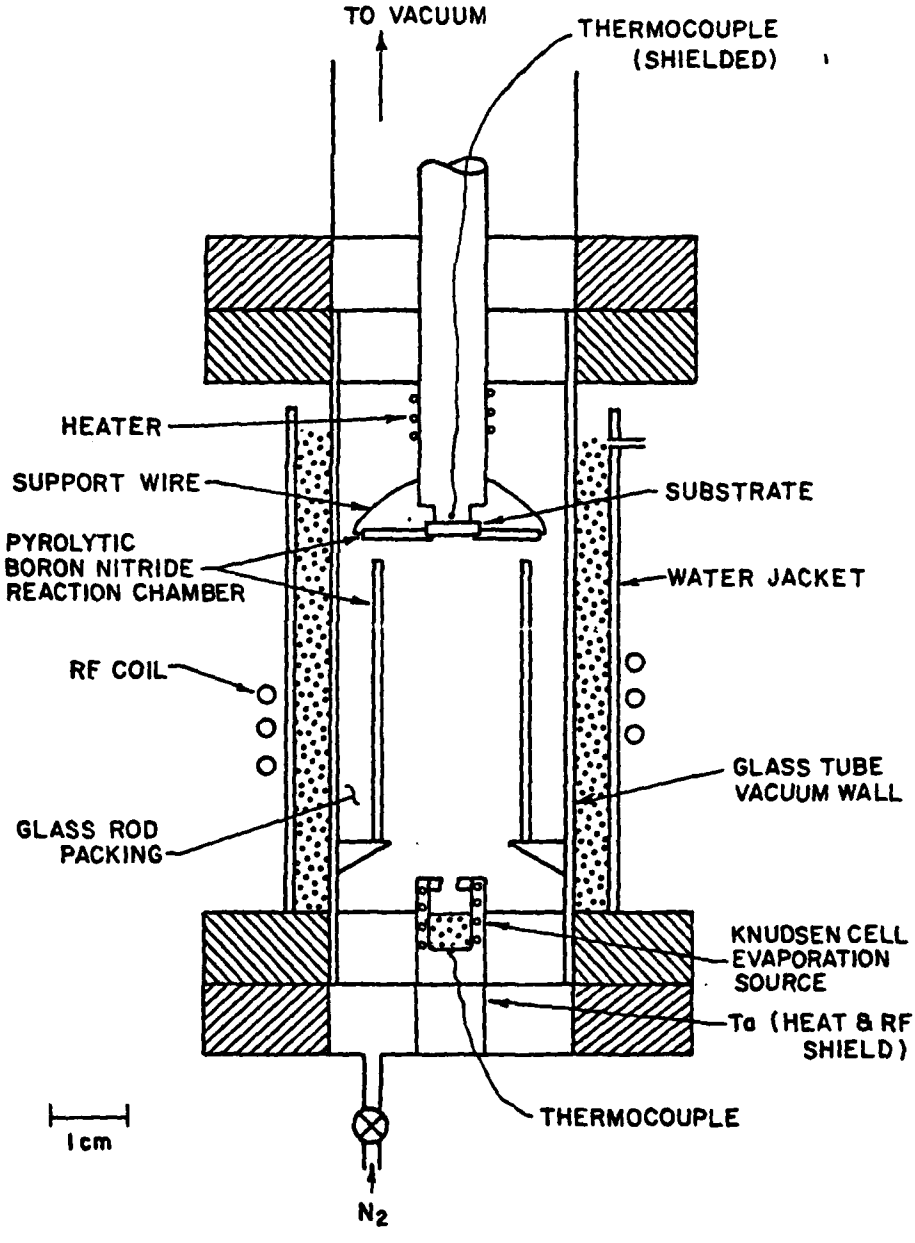

Figure B2. GaN Reactive Evaporator

Figure B3 shows an overall schematic diagram of the ultra-high vacuum system of which the GaN reactor is the central part. Pumping is oil-free, consisting of sorption roughing and sputter-ion UHV pumping to evacuate the system to 10^{-6} Pa prior to each growth run. A second sorption pump is used to pump the large N_2 gas load during growth. N_2 pressure and flow rate through the reaction tube can be controlled independently using the inlet leak valve and outlet throttle valve, with pressure being accurately monitored on a capacitance manometer. RF interference with the process control electronics has been eliminated by thorough shielding of the RF circuit and by the use of RF shunting filters on the temperature feedback loops.

Using this apparatus, a RF discharge was confined first in a sapphire and later in a BN reaction chamber at pressures from 10 Pa to 10^3 Pa of N_2. Although no attempt has been made to work outside this pressure region, it should be possible to do so. A discharge driven by two KW of RF power was demonstrated, but most work has been done with less power.

Figure B3 shows an overall schematic diagram of the ultra-high vacuum system of which the GaN reactor is the central part. Pumping is oil-free, consisting of sorption roughing and sputter-ion UHV pumping to evacuate the system to 10^{-6} Pa prior to each growth run. A second sorption pump is used to pump the large N_2 gas load during growth. N_2 pressure and flow rate through the reaction tube can be controlled independently using the inlet leak valve and outlet throttle valve, with pressure being accurately monitored on a capacitance manometer. RF interference with the process control electronics has been eliminated by thorough shielding of the RF circuit and by the use of RF shunting filters on the temperature feedback loops.

Using this apparatus, a RF discharge was confined first in a sapphire and later in a BN reaction chamber at pressures from 10 Pa to 10^3 Pa of N_2. Although no attempt has been made to work outside this pressure region, it should be possible to do so. A discharge driven by two KW of RF power was demonstrated, but most work has been done with less power.

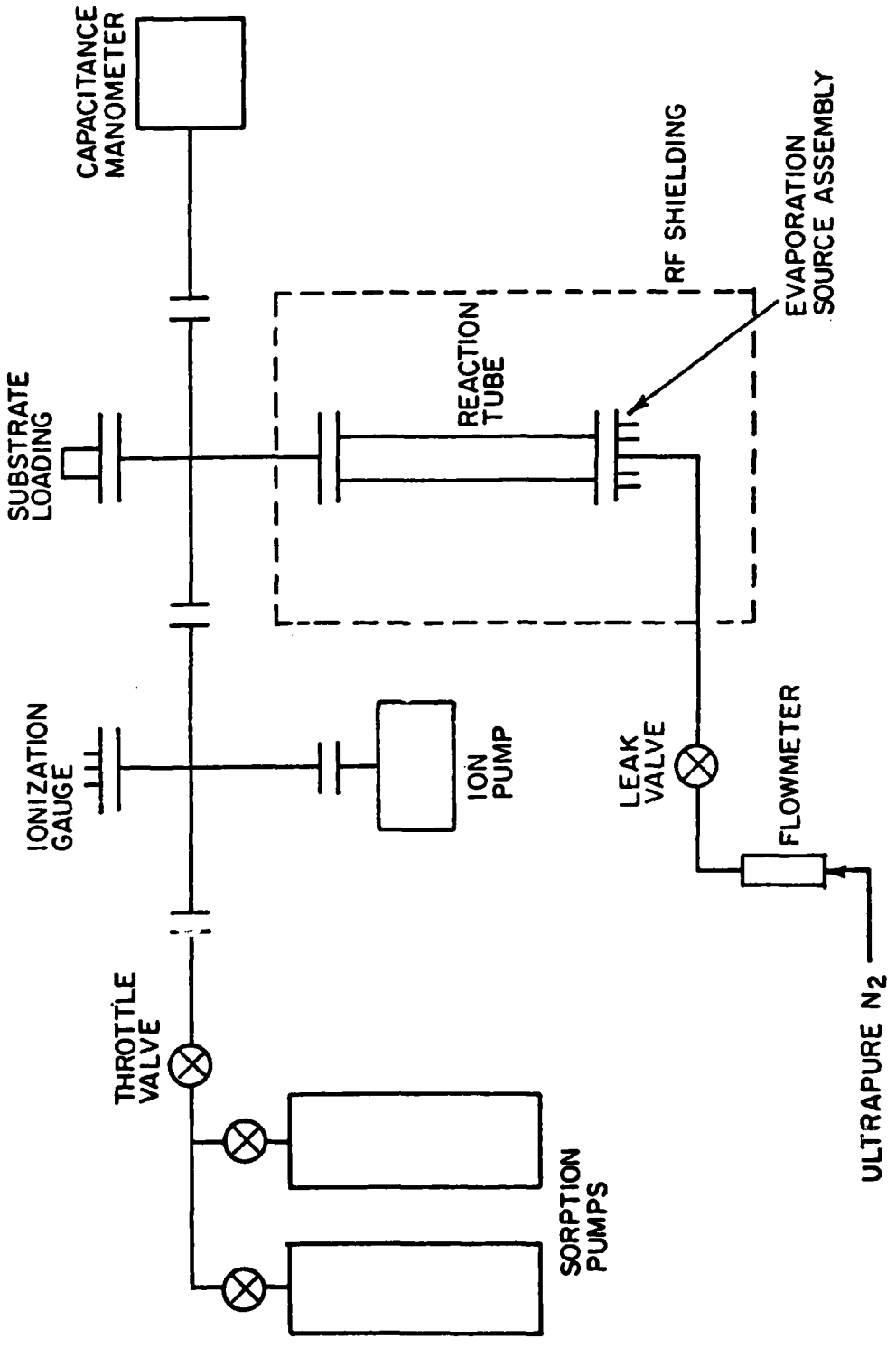

Figure B3. Piping Diagram of GaN Reactor

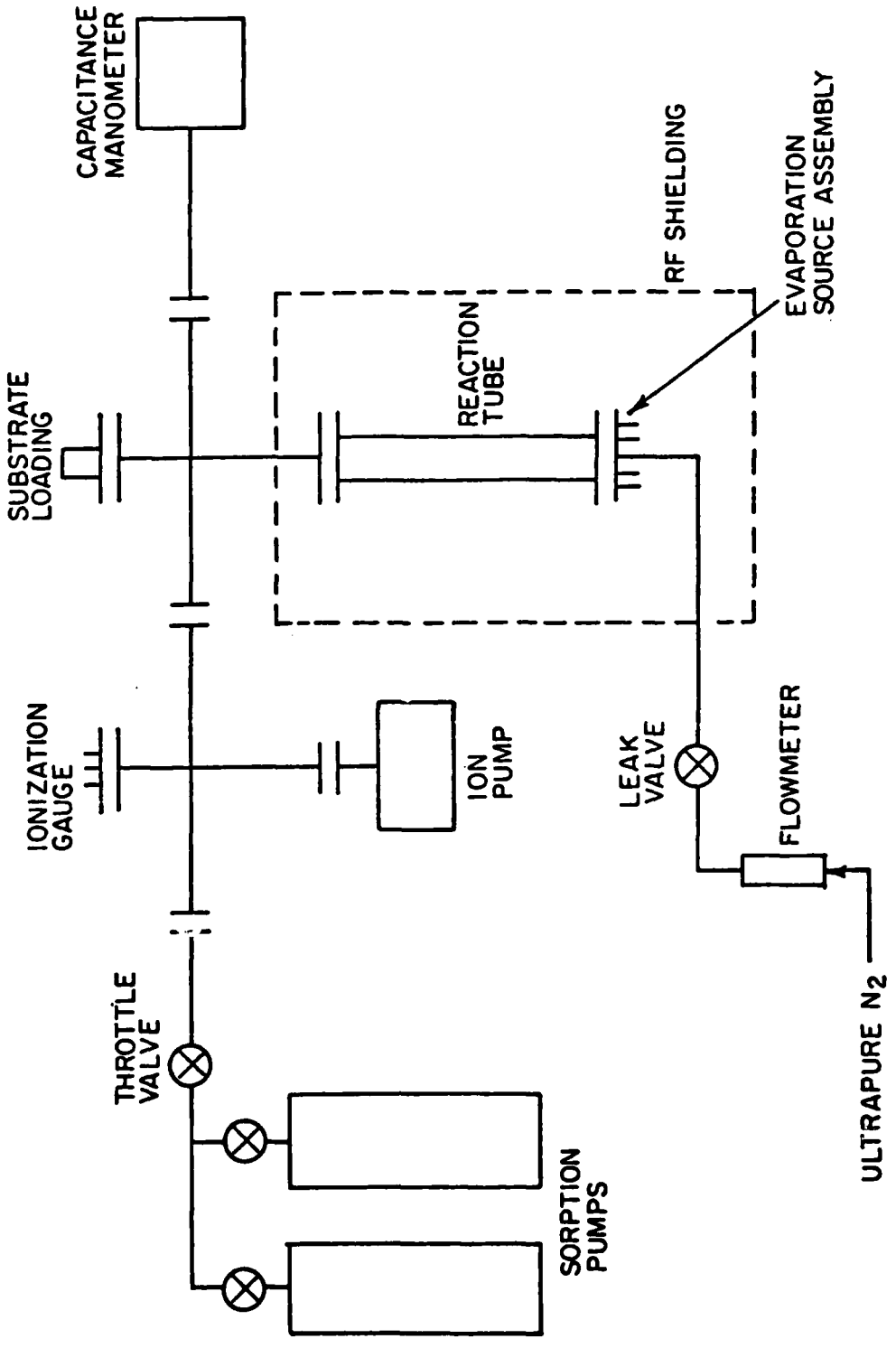

Figure B3. Piping Diagram of GaN Reactor

REPORTS DISTRIBUTION LIST FOR ONR PHYSICS PROGRAM OFFICE
UNCLASSIFIED CONTRACTS

Director — 3 copies
Defense Advanced Research Projects Agency
Attn: Technical Library
1400 Wilson Blvd.
Arlington, Virginia 22209

Office of Naval Research — 3 copies
Physics Program Office (Code 421)
800 North Quincy Street
Arlington, Virginia 22217

Office of Naval Research — 1 copy
Assistant Chief for Technology (Code 200)
800 North Quincy Street
Arlington, Virginia 22217

Naval Research Laboratory — 3 copies
Department of the Navy
Attn: Technical Library
Washington, D. C. 20375

Office of the Director of Defense — 3 copies
Research and Engineering
Information Office Library Branch
The Pentagon
Washington, D. C. 20301

U. S. Army Research Office — 2 copies
Box 12211
Research Triangle Park
North Carolina 27709

Defense Documentation Center — 12 copies
Cameron Station (TC)
Alexandria, Virginia 22314

Director, National Bureau of Standards — 1 copy
Attn: Technical Library
Washington, DC 20234

Commanding Officer — 3 copies
Office of Naval Research Branch Office
536 South Clark Street
Chicago, Illinois 60605

REPORTS DISTRIBUTION LIST FOR ONR PHYSICS PROGRAM OFFICE
UNCLASSIFIED CONTRACTS

Director — 3 copies
Defense Advanced Research Projects Agency
Attn: Technical Library
1400 Wilson Blvd.
Arlington, Virginia 22209

Office of Naval Research — 3 copies
Physics Program Office (Code 421)
800 North Quincy Street
Arlington, Virginia 22217

Office of Naval Research — 1 copy
Assistant Chief for Technology (Code 200)
800 North Quincy Street
Arlington, Virginia 22217

Naval Research Laboratory — 3 copies
Department of the Navy
Attn: Technical Library
Washington, D. C. 20375

Office of the Director of Defense — 3 copies
Research and Engineering
Information Office Library Branch
The Pentagon
Washington, D. C. 20301

U. S. Army Research Office — 2 copies
Box 12211
Research Triangle Park
North Carolina 27709

Defense Documentation Center — 12 copies
Cameron Station (TC)
Alexandria, Virginia 22314

Director, National Bureau of Standards — 1 copy
Attn: Technical Library
Washington, DC 20234

Commanding Officer — 3 copies
Office of Naval Research Branch Office
536 South Clark Street
Chicago, Illinois 60605

Commanding Officer — 3 copies
Office of Naval Research Branch Office
1030 East Green Street
Pasadena, California 91101

San Francisco Area Office — 3 copies
Office of Naval Research
One Hallidie Plaza
Suite 601
San Francisco, California 94102

Commanding Officer — 3 copies
Office of Naval Research Branch Office
666 Summer Street
Boston, Massachusetts 02210

New York Area Office — 1 copy
Office of Naval Research
715 Broadway, 5th Floor
New York, New York 10003

Director — 1 copy
U. S. Army Engineering Research
and Development Laboratories
Attn: Technical Documents Center
Fort Belvoir, Virginia 22060

ODDR&E Advisory Group on Electron Devices — 3 copies
201 Varick Street
New York, New York 10014

Air Force Office of Scientific Research — 1 copy
Department of the Air Force
Bolling AFB, D. C. 22209

Air Force Weapons Laboratory — 1 copy
Technical Library
Kirtland Air Force Base
Albuquerque, New Mexico 87117

Air Force Avionics Laboratory — 1 copy
Air Force Systems Command
Technical Library
Wright-Patterson Air Force Base
Dayton, Ohio 45433

Lawrence Livermore Laboratory — 1 copy
Attn: Dr. W. F. Krupke
University of California
P. O. Box 808
Livermore, California 94550

Commanding Officer — 3 copies
Office of Naval Research Branch Office
1030 East Green Street
Pasadena, California 91101

San Francisco Area Office — 3 copies
Office of Naval Research
One Hallidie Plaza
Suite 601
San Francisco, California 94102

Commanding Officer — 3 copies
Office of Naval Research Branch Office
666 Summer Street
Boston, Massachusetts 02210

New York Area Office — 1 copy
Office of Naval Research
715 Broadway, 5th Floor
New York, New York 10003

Director — 1 copy
U. S. Army Engineering Research
and Development Laboratories
Attn: Technical Documents Center
Fort Belvoir, Virginia 22060

ODDR&E Advisory Group on Electron Devices — 3 copies
201 Varick Street
New York, New York 10014

Air Force Office of Scientific Research — 1 copy
Department of the Air Force
Bolling AFB, D. C. 22209

Air Force Weapons Laboratory — 1 copy
Technical Library
Kirtland Air Force Base
Albuquerque, New Mexico 87117

Air Force Avionics Laboratory — 1 copy
Air Force Systems Command
Technical Library
Wright-Patterson Air Force Base
Dayton, Ohio 45433

Lawrence Livermore Laboratory — 1 copy
Attn: Dr. W. F. Krupke
University of California
P. O. Box 808
Livermore, California 94550

Harry Diamond Laboratories — 1 copy
Technical Library
2800 Powder Mill Road
Adelphi, Maryland 20783

Naval Air Development Center — 1 copy
Attn: Technical Library
Johnsville
Warminster, Pennsylvania 18974

Naval Weapons Center — 1 copy
Technical Library (Code 753)
China Lake, California 93555

Naval Training Equipment Center — 1 copy
Technical Library
Orlando, Florida 32813

Naval Underwater Systems Center — 1 copy
Technical Library
New London, Connecticut 06320

Commandant of the Marine Corps — 1 copy
Scientific Advisor (Code RD-1)
Washington, DC 20380

Naval Ordnance Station — 1 copy
Technical Library
Indian Head, Maryland 20640

Naval Postgraduate School — 1 copy
Technical Library (Code 0212)
Monterey, California 93940

Naval Missile Center — 1 copy
Technical Library (Code 5632.2)
Point Mugu, California 93010

Naval Ordnance Station — 1 copy
Technical Library
Louisville, Kentucky 40214

Commanding Officer — 1 copy
Naval Ocean Research & Development Activity
Technical Library
NSTL Station, Mississippi 39529

Naval Explosive Ordnance Disposal Facility — 1 copy
Technical Library
Indian Head, Maryland 20640

Harry Diamond Laboratories — 1 copy
Technical Library
2800 Powder Mill Road
Adelphi, Maryland 20783

Naval Air Development Center — 1 copy
Attn: Technical Library
Johnsville
Warminster, Pennsylvania 18974

Naval Weapons Center — 1 copy
Technical Library (Code 753)
China Lake, California 93555

Naval Training Equipment Center — 1 copy
Technical Library
Orlando, Florida 32813

Naval Underwater Systems Center — 1 copy
Technical Library
New London, Connecticut 06320

Commandant of the Marine Corps — 1 copy
Scientific Advisor (Code RD-1)
Washington, DC 20380

Naval Ordnance Station — 1 copy
Technical Library
Indian Head, Maryland 20640

Naval Postgraduate School — 1 copy
Technical Library (Code 0212)
Monterey, California 93940

Naval Missile Center — 1 copy
Technical Library (Code 5632.2)
Point Mugu, California 93010

Naval Ordnance Station — 1 copy
Technical Library
Louisville, Kentucky 40214

Commanding Officer — 1 copy
Naval Ocean Research & Development Activity
Technical Library
NSTL Station, Mississippi 39529

Naval Explosive Ordnance Disposal Facility — 1 copy
Technical Library
Indian Head, Maryland 20640

Naval Ocean Systems Center — 1 copy
Technical Library
San Diego, California 92152

Naval Surface Weapons Center — 1 copy
Technical Library
Dahlgren, Virginia 22448

Naval Surface Weapons Center (White Oak) — 1 copy
Technical Library
Silver Spring, Maryland 20910

Naval Ship Research and Development Center — 1 copy
Central Library (Code L42 and L43)
Bethesda, Maryland 20084

Naval Avionics Facility — 1 copy
Technical Library
Indianapolis, Indiana 46218

Naval Ocean Systems Center — 1 copy
Technical Library
San Diego, California 92152

Naval Surface Weapons Center — 1 copy
Technical Library
Dahlgren, Virginia 22448

Naval Surface Weapons Center (White Oak) — 1 copy
Technical Library
Silver Spring, Maryland 20910

Naval Ship Research and Development Center — 1 copy
Central Library (Code L42 and L43)
Bethesda, Maryland 20084

Naval Avionics Facility — 1 copy
Technical Library
Indianapolis, Indiana 46218

Addendum

Prof. Rointan Bunshah
6532 Boelter Hall
University of California
Los Angeles, CA 90024

Dr. Maurice Francombe
Westinghouse Research
Laboratories
Pittsburgh, PA 15235

Dr. Murray Gershenzon
University of Southern
California, University Park
Los Angeles, CA 90007

Dr. Jacques I. Pankove
RCA Laboratories
Princeton, NJ 08540

Dr. James Van Vechten
IBM, Watson Research Center
Yorktown Heights, NY 10598

Dr. David Yaney
Bell Laboratories
Allentown, PA

Addendum

Prof. Rointan Bunshah
6532 Boelter Hall
University of California
Los Angeles, CA 90024

Dr. Maurice Francombe
Westinghouse Research
Laboratories
Pittsburgh, PA 15235

Dr. Murray Gershenzon
University of Southern
California, University Park
Los Angeles, CA 90007

Dr. Jacques I. Pankove
RCA Laboratories
Princeton, NJ 08540

Dr. James Van Vechten
IBM, Watson Research Center
Yorktown Heights, NY 10598

Dr. David Yaney
Bell Laboratories
Allentown, PA

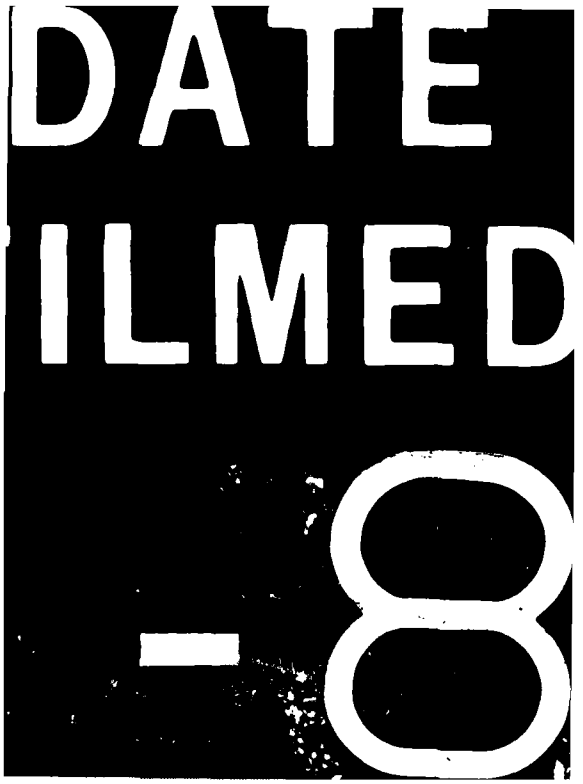
DATE
ILMED
-8

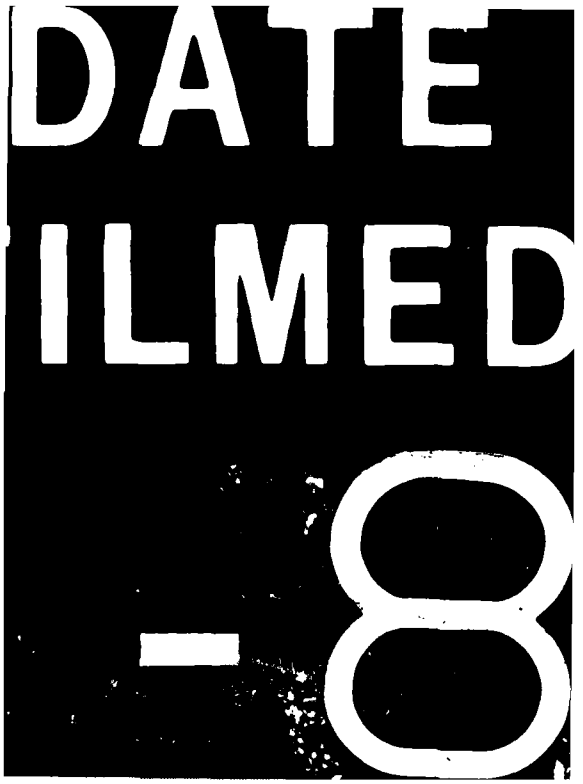
DATE
ILMED
-8